Pergamon

Geochimica et Cosmochimica Acta, Vol. 67, No. 18, pp. 3473–3496, 2003

0016-7037/03 $30.00 + .00

doi:10.1016/S0016-7037(03)00084-X

Quantitative multi-element analysis of minerals, fluid and melt inclusions by laser-ablation inductively-coupled-plasma mass-spectrometry

C. A. HEINRICH,[1,*] T. PETTKE,[1] W. E. HALTER,[1] M. AIGNER-TORRES,[1] A. AUDÉTAT,[1,†] D. GÜNTHER,[2] B. HATTENDORF,[2] D. BLEINER,[2,‡] M. GUILLONG,[2] and I. HORN[2,§]

[1]Isotope Geochemistry and Mineral Resources, Department of Earth Sciences, Swiss Federal Institute of Technology, ETH Zentrum NO, 8092 Zürich, Switzerland

[2]Laboratory for Inorganic Chemistry, Department of Chemistry, Swiss Federal Institute of Technology, ETH Hönggerberg HCI, 8093 Zürich, Switzerland

(*Received March* 13, 2002; *accepted in revised form February* 3, 2003)

Abstract—Laser-ablation ICPMS has become widely accessible as a powerful and efficient multi-element microanalytical technique. One of its key strengths is the ability to analyse a wide concentration range from major (tens of wt.%) to trace (ng/g) levels in minerals and their microscopic inclusions. An ArF excimer laser system ($\lambda = 193$ nm) with imaging optics for controlled UV ablation and simultaneous petrographic viewing was designed specifically for representative sampling and quantitative multi-element analysis of microscopic fluid, melt and mineral inclusions beneath the sample surface. After a review of the requirements and recent technical developments, results are presented which together document the reliability and reproducibility of quantitative microanalysis of complex samples such as zoned crystals or fluid and melt inclusions in various host minerals. Analytical errors due to elemental fractionation are reduced to the typical precision achieved by quadrupole LA-ICPMS in multi-element mode (2–5% RSD). This progress is largely due to the small size of aerosol particles generated by the optimized UV optical system. Depth profiling yields representative and accurate concentration results at a resolution of $\sim$0.1 μm perpendicular to the ablation surface. Ablation is largely matrix-insensitive for different elements, such that silicate and borate glasses, silicates and oxide minerals, or direct liquid ablation can be used interchangeably for external standardization of any homogeneous or heterogeneous material. The absolute ablation rate is material dependent, however, so that quantitative LA-ICPMS analysis requires an internal standard (i.e., an independent constraint such as the absolute concentration of one element).

Our approach to quantifying fluid and melt inclusion compositions is described in detail. Experiments with synthetic fluid inclusions show that accurate results are obtained by combining the LA-ICPMS analysis of element concentration ratios with a microthermometric measurement of the NaCl equivalent concentration and an empirical description of the effect of major cations on the final melting temperatures of ice, hydrohalite or halite. Expected calibration errors for NaCl-H_2O-dominated fluids are smaller than the typical analytical scatter within an assemblage of simultaneously trapped fluid inclusions. Analytical precision is limited by representative ablation of all phases in heterogeneous inclusions and the integration of transient ICPMS signals, to typically $\pm$10 to 20% RSD. Element concentrations in devitrified and even coarsely crystallized silicate melt inclusions can be reconstituted from LA-ICPMS signals. Deconvolution of inclusion and host signals with internal standardization automatically corrects for sidewall crystallization after melt entrapment at high temperature. A test using melt inclusions in a midocean ridge basalt, a summary of published geochemical studies and a new application to REE analysis of coexisting fluids and mineral phases in carbonatite-related veins illustrate the versatility and some of the strengths and limitations of LA-ICPMS, in comparison with other microanalytical techniques.

1. INTRODUCTION

Laser ablation is a powerful and versatile technique for in situ sampling of solid materials for major, trace and isotopic analysis. Its advance into the earth sciences has been closely linked with progress in the development of new laser types over the last decade, from the initial use of visible and infrared wavelengths (Gray, 1985; Perkins et al., 1991, 1993; Jackson et al., 1992; Moenke-Blankenburg et al., 1992, 1994; Pearce et al., 1992; Darke and Tyson, 1993), through the generation of ultraviolet beams by quadrupling or quintupling of Nd:YAG lasers (Jenner et al., 1993; Longerich et al., 1996b, 1997; Nesbitt et al., 1997; Perkins et al., 1997; Jeffries et al., 1998; Günther et al., 1999) to the introduction of excimer lasers producing a short-wavelength beam from a primary UV photon source (Günther et al., 1997a; Sylvester and Ghaderi, 1997; Eggins et al., 1998a, 1998b; Horn et al., 2000). The advance of laser ablation (LA) as a micro-sampling technique for trace-element analysis has paralleled the development of increasingly sensitive and versatile detection capabilities. Inductively coupled plasma mass spectrometry using a quadrupole mass filter (ICPMS unless further specified) has become the main instrumentation for multi-element applications from major to trace-

* Author to whom correspondence should be addressed (heinrich@erdw.ethz.ch); also at the University of Zürich, Faculty of Mathematics and Natural Sciences, 8006 Zürich, Switzerland.
† Present address: Institut für Mineralogie, Universität Tübingen, Wilhelmstrasse 56, D-72074, Tübingen, Germany.
‡ Present address: Eidgenössiche Materialprüfungasanstalt EMPA, Ueberlandstrasse 129, CH-8600, Dübendorf, Switzerland.
§ Present address: Institut für Mineralogie, Universität Hannover, Callinstrasse 3, D-30167, Hannover, Germany.

element levels (Durrant, 1999; Günther et al., 1999, 2000; Sylvester, 2001a). Today, LA-ICPMS is regarded by many geochemists as the most widely applicable and most affordable 'trace-element microprobe', as indicated by a proliferation of grant proposals for new laboratory facilities. A rapid increase of applications are published for materials as diverse as meteorite metals (Hirata and Nesbitt, 1997), major and accessory minerals in igneous and metamorphic rocks (e.g., Suhr et al., 1998; Sha and Chappell, 1999; Poitrasson et al., 2000), volcanic glass shards (Westgate et al., 1994; Bryant et al., 1999), detrital zircons in sediments (Knudsen et al., 2001) and fish bones (Campana et al., 1997).

The potential of LA-ICP optical emission and mass spectrometry for analysing fluid and melt inclusions was recognized by Horn and Tye (1989), Ramsey et al. (1992), Rankin et al. (1992), and Wilkinson et al. (1994). Moissette et al. (1996) and Shepherd and Chenery (1995) were the first to calibrate element ratios in fluid inclusions by comparison of LA-ICPMS signals with emulsions or microcapillaries containing standard solutions with known element ratios. With the advent of new UV lasers and more sensitive mass spectrometers, LA-ICPMS has developed into the first widely accessible microanalytical technique for quantitative analysis of major and trace-element concentrations in single fluid inclusions (Günther et al., 1998; Loucks and Mavrogenes, 1999), leading to a wide range of geochemical applications to experimental and natural fluid systems.

Despite numerous publications describing the development and application of LA-ICPMS, important tests of accuracy and precision with comparable rigor to those applied to other microanalytical techniques are still missing. The aim of this contribution is to quantify some of the strengths of LA-ICPMS and to identify its main limitations, as they emerged from extensive testing of an excimer laser system developed at ETH Zürich and its comparison with other instruments. We summarize the key aspects of our approach to quantitative multi-element microanalysis of homogeneous and heterogeneous materials. Test experiments were designed to assess the precision and to verify the accuracy of LA-ICPMS quantification for heterogeneous samples such as fluid and melt inclusions in minerals.

This paper is composed of three major parts. In a first part on basic processes and instrumentation, a short review of the working principles of LA-ICPMS and recent instrumental developments is followed by a discussion of the ablation process, the problem of elemental fractionation and the role of interferences in LA-ICPMS, which may be more important than often appreciated. In the second part, the principles and practice of quantification are reviewed and tested with applications to in situ micro-sampling for quantitative analysis of major to trace-element compositions of solid materials. Verification of representative spatial sampling, including depth-profiling perpendicular to a sample surface, and the accuracy of matrix-independent calibrations are essential prerequisites for quantitative analysis of heterogeneous samples, such as multiphase inclusions inside a mineral. In the third part, the methods and reliability of quantitative analysis of fluid and melt inclusions in minerals are discussed and tested in detail. Here, LA-ICPMS has a unique advantage due to its ability, with appropriate instrumentation, to reconstruct the bulk composition of fluids and melts that have separated into several phases after trapping at high temperatures and pressures. The practical approach to fluid and melt inclusion analysis, the accurate quantification of signals, and the estimation of associated uncertainties are discussed, using a range of typical applications. An outlook of future developments in multi-element and trace geochemistry of mineral materials by laser-ablation microanalysis, in comparison with other techniques, concludes the paper.

2. PROCESSES AND INSTRUMENTATION

2.1. Principle and Essential Requirements

The general layout of a LA-ICPMS microprobe system is shown in Figure 1, including some of the key features of the ETH prototype system (Günther et al., 1997a) from which the commercially available GeoLas system has emerged (Microlas, Göttingen, Germany). Successful microanalytical work depends on three instrument components, which ideally perform the following key functions: (1) A pulsed laser beam and optical components allowing representative removal of sample material from a selected spot on the sample surface; (2) a sample cell flushed by a continuous stream of a carrier gas taking up the ablated material in the form of a fine aerosol and transporting these particles without element-selective loss to the inductively coupled plasma for complete vaporization and ionization; and (3) a fast and sensitive detection system permitting acquisition of representative multi-element data from short transient signals over a large range of masses and intensities, with minimal instrumental background for all elements of interest.

2.2. Lasers and UV/Visible Optical Instrumentation

The physical process of 'laser ablation' depends on the mechanisms of absorption and dissipation of laser energy in the target material. Key characteristics of irradiation include laser wavelength, pulse width (duration), and the density and lateral distribution of laser energy delivered onto the sample surface. The coupled effects of these parameters on analytical performance are still not fully understood.

Two types of lasers are widely used for ablation analysis today. Solid-state lasers generally use a Nd:YAG infrared laser whose primary wavelength of 1064 nm is reduced to harmonics in the ultraviolet range, by frequency quadrupling to 266 nm or quintupling to 213 nm. Excimer lasers use the primary UV photons emitted by an excited dimer in a gas mixture, such as XeCl (308 nm), KrCl (248 nm), ArF (193 nm) or F_2 (157 nm). In most geochemical applications, UV radiation ($<\sim$300 nm) was found to be superior to visible and infrared (Jeffries et al., 1996), where ablation mainly occurs by mechanical spalling or by thermal melting and sputtering of melt droplets (Moenke-Blankenburg and Günther, 1992; Moenke-Blankenburg et al., 1992; Darke and Tyson, 1993). Theoretical considerations comparing UV photon energies with typical bonding energies in silicates suggest a fundamental change in ablation mechanism from dominantly thermal heating by the longer UV wavelengths ($\sim$250–300 nm) to 'cold' ablation by breaking of chemical bonds below $\sim$200 nm (Wiechert and Hoefs, 1995; Fiebig et al., 1999). Jeffries et al. (1998) reported an improvement in ablation behavior using 213 nm instead of 266 nm, but

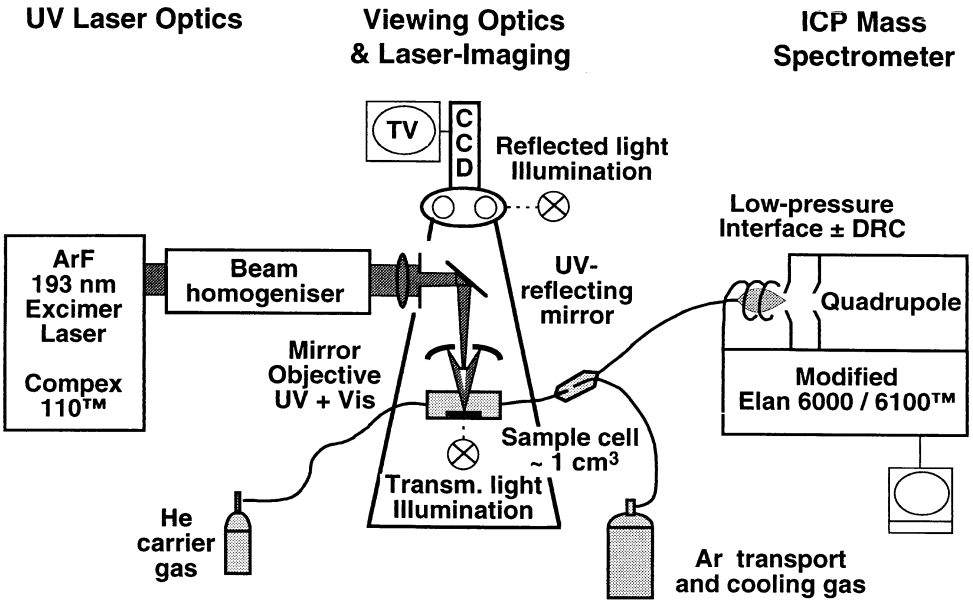

Fig. 1. Layout of the laser-ablation ICPMS instrument developed at ETH Zürich. Optical homogenisation of the primary UV beam (Fig. 2) and helium as carrier gas are not universally used in other LA-ICPMS laboratories, but seem to be important for many applications reported in this paper.

Liu et al. (2000) and Russo et al. (2000) found the differences between these shorter and longer UV wavelengths less conclusive. Comparative tests under near-identical transport and ICP conditions show a clear improvement in the efficiency of aerosol uptake and signal smoothness with the use of an 193-nm excimer system, compared with a commercial 266-nm Nd:YAG laser system (Günther and Heinrich, 1999b).

The optical components delivering the laser light onto the sample surface are at least as important for stable ablation as the laser wavelength. With its combined 193-nm UV imaging and visual observation optics using an objective with high numerical aperture (Fig. 2), this system delivers an adjustable and laterally homogeneous energy density on the sample (fluence; 2–35 J cm^{-2} per pulse), independent of crater diameter (4–120 μm). Controlled ablation of ~0.1 μm per shot on sapphire (Guillong and Günther, 2001) or quartz was achieved with the beam-homogenising optics using a typical fluence of ~10 J cm^{-2} per pulse. Tests with a similarly homogenized optical system using a high-power 266-nm Nd:YAG laser also yielded encouraging results, indicating that the wavelength may not be the single most important factor for successful laser ablation (Horn et al., 2001; Guillong et al., 2002).

The optical setup shown in Figure 2 allows 'layer-by-layer' ablation from a flat-bottomed crater, while simultaneously allowing visual observation through a modified petrographic microscope. It uses a single dispersion-free mirror objective (Schwarzschild type) with high numeric aperture, allowing excellent on-line viewing and ablation. Flat-bottomed craters can be ablated only to a depth approximating their top diameter, because of the convergent laser beam path generated by the high numeric aperture of the objective. The resulting conical crater shape of limited depth is the main difference in comparison with other excimer ablation systems (Eggins et al., 1998a; Horn et al., 2000). As a result of the optical path and the downward decreasing crater diameter, our LA-ICPMS signals are smooth but intensities decrease uniformly with time (Fig. 3). The imaging (rather than focusing) optics also allow rapid variation of crater diameters at constant UV energy density on the sample, by switching of an aperture behind the field lens. This facility is the key to complete and representative ablation of fluid inclusions (below).

2.3. Sample Cells and Aerosol Transport

The volume of the sample cell is the most influential parameter in terms of aerosol dispersion along the transport path from the ablation site to the plasma. Together with the length and diameter of the transport tubes, the cell volume primarily affects the time attenuation and shape of the transient ICPMS signal resulting from a short ablation event. The cell volume can be used to influence the sample density in the plasma and therefore the signal-to-noise ratio in the ICPMS signal. Quadrupole ICPMS instruments record transient signals sequentially, by cycling through all masses of interest and measuring each for a short period (the 'dwell time', typically 10–100 ms). Multi-element analysis of a limited amount of sample material demands a trade-off between signal intensity and signal duration, for optimal quantification of integrated intensities. A large cell volume (e.g., 20–100 cm^3) leads to relatively long signals of low intensity, permitting a greater number of measurements on each element over the duration of the signal, and thus a potentially more representative and reproducible analysis. A small sample cell (e.g., 1–5 cm^3 as typically used for fluid and melt inclusion analysis) leads to shorter signals and higher signal-to-noise ratios at a given mass of analyte. This improves the detection limits but reduces representative sampling, which may lead to less reproducible analyses. Using typical parameters for data acquisition of a transient signal (with ~10 ms

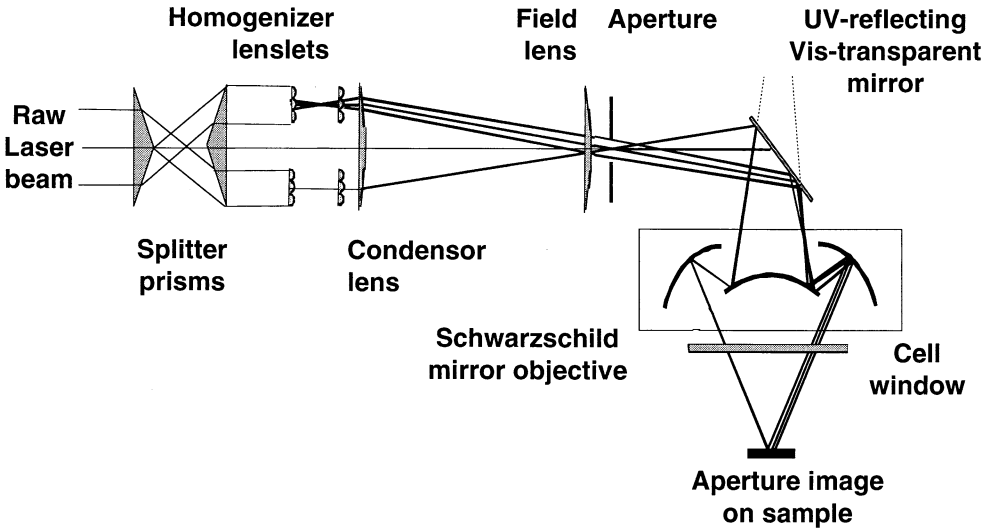

Fig. 2. Optical beam path of the ETH Zürich/GeoLas prototype (Günther et al., 1997a), combining homogenized UV ablation with simultaneous high-quality visual observation of the sample. An ArF excimer laser (Compex 110, Lambda Physik) provides pulses of up to 200 mJ at a wavelength of 193 nm. The primary beam, with roughly rectangular 10 × 25 mm cross-section, is first divided by two prisms into two equal parts of parallel laser light, then passes through two arrays of 18 × 18 cylindrical lenslets, which together with a condenser lens concentrate the laser light from 324 initial segments into a single homogeneously illuminated area of ~3 × 3 mm. An aperture of any desired size or shape cuts out a portion of this area, which is then imaged by a 25× demagnifying mirror objective onto the sample surface. This imaging-optical system delivers a laterally homogeneous distribution of UV intensity on the sample surface. The size of the ablation spot can be changed instantaneously by switching the aperture mask, while maintaining equal energy density on the sample surface. A UV-reflecting dielectric mirror, transparent to visible light, is located between the aperture and the objective, allowing excellent on-line viewing by CCD camera in transmitted or reflected light.

dwell time on each element) requires at least 10 to 15 sampling cycles. Fewer measurements on each element not only lead to poor signal definition but can also result in systematic errors (Pettke et al., 2000). This places a practical lower limit on useful signal durations (a few seconds) and sample cell volumes (~1 cm^3) for quantitative multi-element analysis by quadrupole ICPMS. Compared with the volume of the sample cell, its shape is of secondary importance, provided that highly turbulent flow throughout the cell is maintained by a small gas injection nozzle (Bleiner and Günther, 2001).

The fraction of the ablated crater mass reaching the ICP as aerosol particles is difficult to quantify. Transport efficiency appears to be limited primarily by re-deposition of sample material immediately around the crater. This loss of analyte cannot be significantly reduced by modifications in cell design or gas-flow geometry (Bleiner and Günther, 2001), but it strongly depends on the type of gas in the sample cell. Helium reduces the amount of material condensed back onto the sample surface and improves signal intensities approximately threefold (Fig. 1; Eggins et al., 1998a; Günther and Heinrich, 1999a). This is not due to a higher ablation rate, but rather reflects an improvement in aerosol uptake in He (Horn et al., 2001), notably in combination with 193-nm ablation. Each laser pulse generates a transient micro-plasma immediately above the ablation spot, which can expand more freely into the He gas due to its lower density and viscosity compared with Ar. As a result, condensation of small particles from the micro-plasma is enhanced and their redeposition onto the sample surface is reduced (Callies et al., 1998), leading to efficient transport of predominantly small aerosol particles (mostly <1 μm; Günther and Heinrich, 1999a) and smooth ICPMS signals (Figs. 4a and 4b).

2.4. Representative Sampling and Minimized Element Fractionation

The key to quantitative analysis and accurate determination of element ratios by LA-ICPMS is the ablation, transport, excitation and detection of a representative aliquot of the sample. Deviations from this requirement are collectively called 'elemental fractionation'. The most obvious evidence of fractionation is a time-dependent variation of intensity ratios for different elements during the ablation of a homogeneous sample (Fig. 4a). The index of time-dependent fractionation has been defined by Fryer et al. (1995), by dividing a transient signal into two equal time segments and comparing element intensity ratios between these (Fig. 4c). Time variations in the elemental intensity ratios affect analytical results, if the sample and the reference material show significantly different fractionation behavior. On the other hand, time-constancy of intensity ratios does not prove that fractionation is absent, and is no guarantee for accurate results because elements in different materials may fractionate to variable degrees (Longerich et al., 1996a). How and where fractionation occurs is still debated, but of central importance to successful LA-ICPMS analysis.

Fractionation may occur at the ablation spot, and can be influenced by laser parameters including wavelength, fluence and lateral energy distribution, pulse repetition rate, focal length of the objective, and focus position relative to the sample (Fryer et al., 1995; Jeffries et al., 1996; Longerich et al., 1996a;

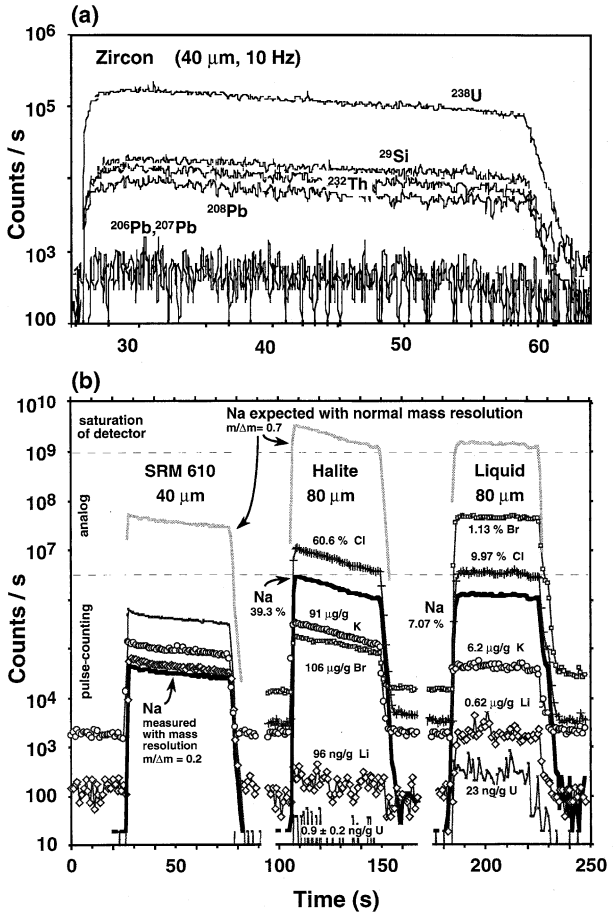

Fig. 3. Time-resolved laser-ablation signals of homogeneous materials (zircon, SRM610 standard glass from NIST, a natural halite crystal, and an aqueous solution ablated through the wall of a polyethylene capillary, as recorded on a Perkin Elmer-SCIEX Elan 6000 or 6100 ICPMS. (a) Thirty-second spot ablation of a homogeneous natural zircon, showing the parallel decrease in all intensities during the ablation of a conical but flat-bottomed crater (40 μm top diameter, ~30 μm deep), generated by the UV imaging optics shown in Figure 2. (b) Three successive signals demonstrating the huge range of intensities and concentrations accessible by dynamic combination of pulse counting and analog detection. Further extension of the concentration range for Na is achieved by selective increase of mass-resolution on ^{23}Na from the standard resolution of 0.7 a.m.u. (used with all other isotopes) to 0.2 a.m.u. This results in a ~1200-fold reduction of ^{23}Na sensitivity (black lines) compared to that expected without selective sensitivity suppression (light gray lines). As Na is often the dominant solute cation, low backgrounds and high dynamic range for Na without loss of sensitivity for trace-elements are essential for quantitative analysis of fluid inclusions.

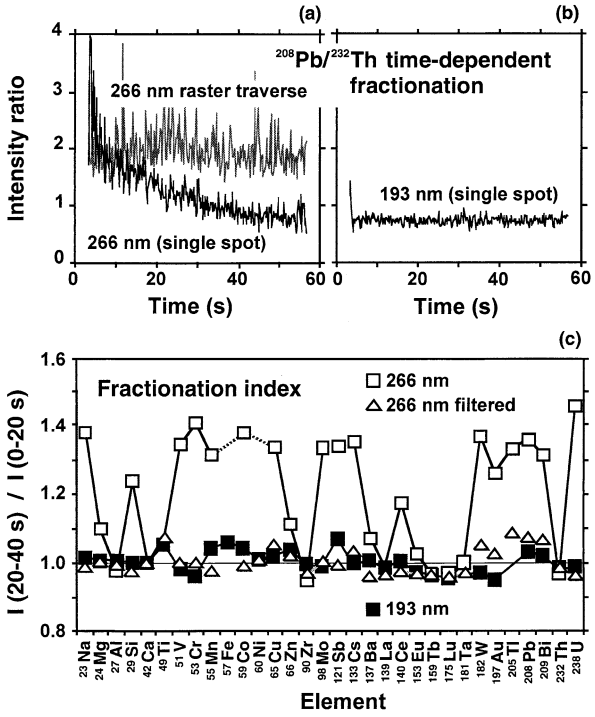

Fig. 4. Experiments summarizing the effects and likely causes of elemental fractionation in UV laser ablation ICPMS, using SRM612 standard glass from NIST (modified from Guillong and Günther, 2002). (a, b) Transient signals for Th and Pb exhibit strong (a: Cetac LSX200, 266-nm Nd:YAG) and undetectable (b: GeoLas, homogenized 193-nm excimer) time-dependent fractionation during ablation under otherwise identical instrument conditions. Variations of the Pb/Th intensity ratio in (a) deviating from the smooth value shown in (b) can be explained by the presence of particles that are too large for complete vaporization and ionization in the ICP. (c) Time-dependent fractionation indices (for total ablation lengths of 40 s; Fryer et al., 1995) ratioed to Ca, illustrating which elements can be affected by element fractionation. Filtering out the large aerosol particles reduces the large fractionation effects with 266 nm (open squares) to much lower values (open triangles). These are comparable to those obtained, without any filtering, using the homogenized 193-nm system (full squares).

Eggins et al., 1998a; Figg et al., 1998; Günther and Heinrich, 1999b; Mank and Mason, 1999; Horn et al., 2000; Russo et al., 2000). Reduction in wavelength from 1064 (IR) to 266 nm or its fifth harmonic at 213 nm (Jeffries et al., 1998) and excimer lasers with 193 nm (Eggins et al., 1998a; Günther and Heinrich, 1999b; Horn et al., 2000) have successively reduced fractionation, now approaching the limits of significance in ICP quadrupole mass-spectrometry. The 193-nm laser, in combination with homogenization optics delivering 'flat top' beam profiles through a high numerical aperture objective (Fig. 2) and helium as carrier gas, yields smooth signals with minimal time-dependent fractionation (Günther and Heinrich, 1999b; Figs. 3a and 4b), to at least a crater depth of one crater diameter. Eggins et al. (1998a) and Horn et al. (2000) reported still measurable fractionation using the same laser wavelength but generally deeper craters resulting from different optical setups. Based on detailed investigation of ablation craters, Eggins et al. (1998a) suggested that fractionation mainly occurs at the ablation site due to partial recondensation of analyte melt onto the ablation surface and the crater walls.

Recent experiments, however, show that fractionation can also occur by incomplete vaporization and ionization of particles in the inductively coupled plasma, and that this effect may dominate the fractionation phenomena observed with different UV laser systems (Fig. 4). Fractionation occurring in the ICP is indirectly affected by the ablation process, by controlling the particle-size distribution in the aerosol. The reduction in time-dependent fractionation shown in Figure 4b (193 nm, homogenized) compared with Figure 4a (266 nm, commercial system)

can be explained by a predominance of small aerosol particles generated by 193-nm ablation in helium, which also leads to a three-fold signal enhancement. More conclusive evidence for particle-induced fractionation in the ICP comes from experiments using particle filtering (Guillong and Günther, 2002) and combinations of one ablation system with different ICP-MS instruments (Günther, 2002).

Figure 4a illustrates the gradual decrease of the U/Th intensity ratio with single-spot ablation by 266 nm, eventually approaching the more constant value obtained with 193 nm ablation in He (Fig. 4b). The constancy of the intensity ratio in Figure 4c results from the generation or transportation of consistently small particles below $\sim$1 μm throughout the duration of 193-nm ablation in He, which allows complete vaporization and excitation of the entire aerosol in the ICP. The greater scatter at initially higher U/Th ratios produced by 266 nm (Fig. 4b) reflects a predominance of larger particles, especially at the beginning of the ablation process. From these larger particles, the relatively volatile Pb may be liberated and ionized in preference over the more refractory Th, some of which remains locked up in residual particles. Filtering out the larger particles with glass-wool inserted into the transfer tubing between sample chamber and ICP leads to lower absolute intensities, but to U/Th ratios with 266 nm that are similar to those obtained with 193-nm ablation (compare open squares and triangles in Fig. 4c; Guillong and Günther, 2002). A direct comparison of one ablation system coupled to two different ICP mass spectrometers operating at somewhat different plasma temperatures (Günther, 2002) confirms that particle-size dependent fractionation mainly occurs in the inductively coupled plasma (Guillong and Günther, 2002), rather than by melt recondensation at the ablation site as previously considered (Eggins et al., 1998a). Figure 4a also illustrates that rastering can produce relatively time-constant, but systematically biased signal ratios, which may lead to incorrect analyses if the fractionation behavior of sample and standard differ (e.g., Hirata and Nesbitt, 1995). It should be noted, however, that these studies have been carried out on silicates and may not apply to all other matrices.

2.5. ICP Mass Spectrometers and the Problem of Interferences

Three main issues determine the type of mass spectrometer best suited for a particular analytical application. The first is the sequential versus simultaneous acquisition of intensities for the masses of interest, which affects the precision (reproducibility) of intensity ratios between different masses, because of the inherent 'flicker' of ICP sources (Fig. 3a). The second is the usable dynamic range of the mass spectrometer, in terms of minimum to maximum recordable intensity, and the mass range that can be accessed within a short time interval (Fig. 3b). Spectral interferences are the third major issue in ICPMS, one that is often underestimated in routine applications (Hieftje et al., 1997; Hattendorf and Günther, 2001; Mason, 2001).

Spectral interferences originating from the plasma gas only (Ar, O, N, C, H ions and ion clusters) result in elevated but time-independent background signals on certain masses. These are corrected by background subtraction from the analyte signal, but may severely degrade the detection limit for certain elements, such as $^{40}Ca^+$ due to the high background by $^{40}Ar^+$, and $^{56}Fe^+$ due to the $^{16}O^{40}Ar^+$ ion cluster. More critical are interferences resulting from polyatomic ions created from elements in the sample matrix, because their intensity co-varies with the intensity of the ablation signal. In many cases, judicious selection of analyte isotopes can circumvent the problem, although often at the expense of optimal detection limit (e.g., the use of ^{65}Cu in Na-rich inclusions, instead of the more abundant ^{63}Cu which may be interfered by $^{40}Ar^{23}Na^+$). In other cases, especially with mono-isotopic elements, corrections must be made based on known isotopic abundances. For example, the $^{40}Ar^{35}Cl^+$ interference on $^{75}As^+$ can be assessed and possibly subtracted by measuring the analyte signal of $^{40}Ar^{37}Cl^+$ and a determination of the intensity ratios on masses 75 and 77 using a Cl-rich but As-free material, such as a pure halite.

Quadrupole mass spectrometers record elements sequentially, but most modern ICPMS instruments have quadrupole settling times as short as 0.2 ms in pulse counting mode, allowing quantification of short ($<$10 s) transient signals with up to 40 elements at a useful precision. Accurate quantification of LA-ICPMS data is based on internal standardization (see below), which commonly requires that major, minor and trace-elements are measured in a single spot analysis. Quadrupole-based ICPMS instruments combine high sensitivity with a very large dynamic range, which is linear over $>$ 8 orders of magnitude with correct cross-calibration of the dual detector (pulse-counting and analog; Fig. 3b). Some instruments enable further extension of the measurable concentration range, by element-specific adjustment of mass resolution. Increasing the resolution ($m/\Delta m$) reduces transmission efficiency, which can be useful for an internal standard element whose intensity would normally exceed the dynamic range of the detector, as illustrated for Na in Figure 3b. Different ICPMS instruments have different sensitivity (response) curves from low to high masses and for wet (solution aspiration) and dry plasmas (LA, desolvating nebulizer). Differences in instrument background, especially for easily ionized matrix elements, may be critical for certain geochemical applications. The use of 'cold plasma' conditions helps in some cases but generally leads to an enhanced formation of polyatomic oxides ions from refractory elements, resulting in a deterioration of sensitivity and increasing number of interferences (especially for the REEs; Tanner, 1995; Wollenweber et al., 1999; Shepherd et al., 2000).

A promising development for overcoming interferences and increasing ion transmission in quadrupole mass spectrometers are multipole ion guides placed in front of the mass filter, such as collision cells (Boulyga and Becker, 2001; Mason, 2001) and dynamic reaction cells (DRC; Tanner and Baranov, 1999a, 1999b; Tanner et al., 2000; Bandura et al., 2001). Collisional focusing leads to a mass-dependent increase in ion transmission and better analyte sensitivity, due to a reduction of the spread of kinetic energies of the ions through collisions with a non-reactive buffer gas (Tanner and Baranov, 1999a; Boulyga and Becker, 2001). With dynamic reaction cells, ion-molecule reactions can be used to selectively attenuate the abundance of an interference in the mass spectrum. A multipole ion guide is used to stabilize the ions within a reaction volume to which the reacting gas is continually supplied. Depending on collision frequency and the thermodynamic and kinetic properties of the species involved, a remarkable 'chemical' resolution between

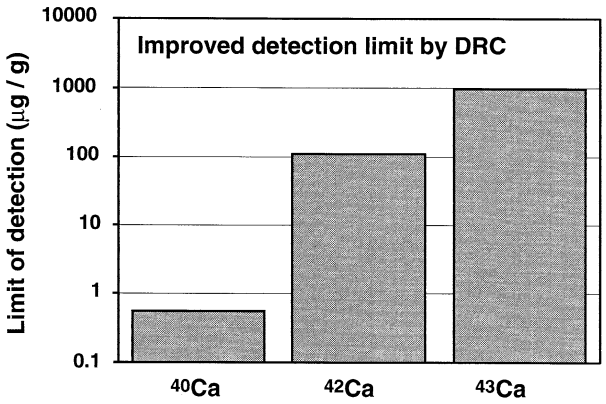

Fig. 5. Improved limits of detection for three Ca isotopes using the dynamic reaction cell (DRC) technology, with H_2(g) as the reactive gas and Ne to thermalize the ions (Hattendorf and Günther, 2000). Minimization of the background signal on $^{40}Ar^+$ lowers the limits of detection by a factor of ~300 compared to the use of mass 42 in normal quadrupole ICPMS (40-μm crater, 10-Hz repetition rate, NIST SRM 610 glass standard).

interfering species can be achieved. Isobaric interference of $^{40}Ar^+$ with $^{40}Ca^+$ can be practically eliminated using either NH_3 or H_2 as reaction gas in an ICPMS equipped with a dynamic reaction cell. Thus the limits of detection for Ca can be improved by $>$ 2 orders of magnitude (Fig. 5), and many polyatomic interferences involving Ar^+ can be significantly reduced. It must be recognized however, that the reactive gas can also lead to the formation of unwanted new polyatomic ions. The DRC technology has not yet been fully tested in routine analysis of geological samples. In multi-element analysis of fast transient signals, H_2 was found to be the most promising reaction gas, leading to minimal formation of additional polyatomic ions, while achieving good chemical resolution from Ar-based interferences (Hattendorf and Günther, 2000; Hattendorf et al., 2001).

High-resolution ICPMS using fast-scanning sector-field magnets allows resolution of certain polyatomic interferences (Shibuya et al., 1998; Cullen et al., 2001). With spectral resolutions of 2000 to 14,000 atomic mass units per mass (m/Δm), polyatomic interferences such as $^{40}Ar^{16}O^+$ on $^{56}Fe^+$, $^{40}Ar^{35}Cl^+$ on $^{75}As^+$, $^{40}Ar^{13}C^+$ on $^{53}Cr^+$ and $^{16}O_2{}^+$ on $^{32}S^+$ can be resolved. Increase in mass resolution reduces acquisition speed and sensitivity and therefore limits laser applications with transient data acquisition, but some of the available instruments are very sensitive in low-resolution mode and almost as fast as quadrupole instruments in recording multi-element spectra. The great potential of combining sector-field instruments with laser ablation is only emerging (Ghazi et al., 2000; Axelsson and Rodushkin, 2001; Latkoczy and Günther, 2002).

Quasi-simultaneous multi-ion sampling of up to 78 isotopes is possible by time-of-flight mass spectrometry (ICP-TOF-MS; Mahoney et al., 1996; Hieftje et al., 1997; Vanhaecke et al., 1999; Bleiner et al., 2000b). This offers a potential advantage for precise determinations of isotope ratios in solution, or for rapidly varying signals such as those obtained from fluid inclusions (Fig. 6). The reproducibility in signal intensity ratios of major elements from laser ablation of solids is better than 2% RSD. Unfortunately, the sensitivity of the instruments available so far is much lower than that of quadrupole-based ICPMS (Bleiner et al., 2000a). Limits of detection in laser-ablation ICP-TOF-MS analysis of solids are near 1 to 10 μg/g for a large 80-μm crater diameter, which is 2 to 3 orders of magnitude poorer than with quadrupole ICPMS. This severely restricts geochemical applications.

Multiple collector–inductively coupled plasma mass spectrometry (MC-ICPMS) is the most suitable instrumentation for high-precision determinations of isotope ratios, although many useful applications of U-Th-Pb and Pb isotope ratios have been made with single collector instruments. Important progress in this field has been reviewed by Halliday et al. (1998), Becker and Dietze (2000), and Jackson et al. (2001). Several applications in combination with laser ablation have been presented (Christensen et al., 1995; Griffin et al., 2000; Stirling et al., 2000; Davidson et al., 2001; Hirata, 2001; Hirata and Ohno, 2001; Machado and Simonetti, 2001; Willigers et al., 2002) and the interested reader is referred to this rapidly growing literature.

3. CALIBRATION FOR MULTI-ELEMENT ANALYSIS OF SOLID MATERIALS

3.1. Internal and External Standards

Absolute ablation efficiency (grams of material ablated per second) varies between different materials and as a function of laser parameters, such as energy density on the sample and pulse rate. It also depends on crater size, which the user may want to vary from spot to spot, to optimize textural control in a series of in situ analyses. Instrumental conditions of the ICPMS can be stabilized over hours of one analytical session, but are not precisely reproducible between sessions. The large number of instrumental variables affecting the overall sensitivity (S_i, the count rate on the mass spectrometer per concentration unit of an element i in a target material) makes absolute calibration of LA-ICPMS analysis impractical. High-quality analysis of an unknown sample (SAMP) by LA-ICPMS therefore uses not only an external standard (STD, a material with known concentrations of all elements of interest), but also one reference element (an internal standard element, r) whose concentration is known independently in the sample and the external standard. This leads to the basic relationship of LA-ICPMS quantification (Longerich et al., 1996b):

$$\frac{C_i^{\mathrm{SAMP}}}{C_r^{\mathrm{SAMP}}} = \frac{C_i^{\mathrm{STD}}}{C_r^{\mathrm{STD}}} \cdot \frac{I_i^{\mathrm{SAMP}}\, I_r^{\mathrm{STD}}}{I_r^{\mathrm{SAMP}}\, I_i^{\mathrm{STD}}} \cdot \underbrace{\frac{S_i^{\mathrm{SAMP}}\, S_r^{\mathrm{STD}}}{S_r^{SAMP}\, S_i^{\mathrm{STD}}}}_{=1} \qquad (1)$$

where C refers to the concentration of the subscripted element (r is a reference element or internal standard, i is unknown elements) in the superscripted material, and I refers to the corresponding background-corrected signal intensity in counts per second (counts/s). In the absence of element-specific fractionation, the sensitivity ratios $S_i^{\mathrm{SAMP}}/S_i^{\mathrm{STD}}$, although numerically unknown, are identical for all elements including the reference element, such that the S terms cancel. This allows the solution of Eqn. 1 for all C_i^{SAMP}, provided that C_r^{SAMP} and the concentrations of all elements in the standard STD are known.

In practice, each signal acquisition is preceded by a mea-

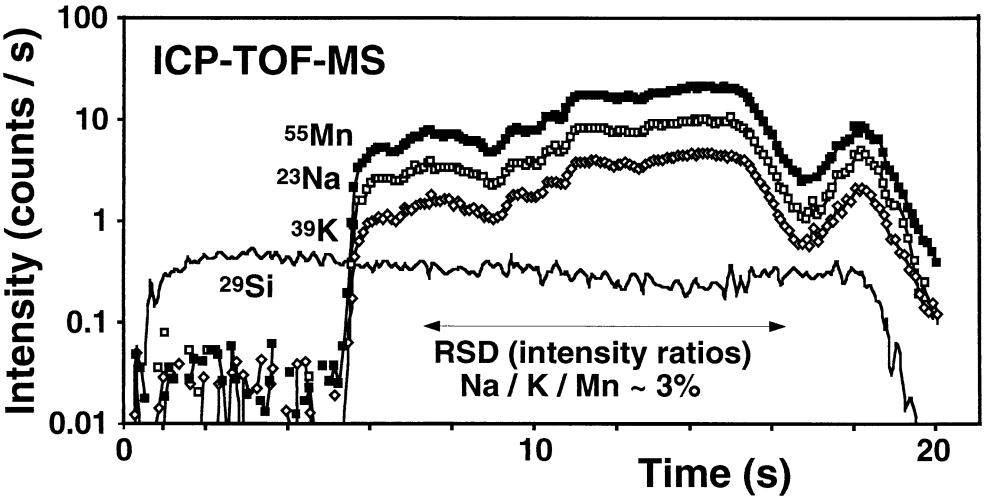

Fig. 6. Transient ICP-time-of-flight-MS signal of Na, K and Mn from the aqueous part of a fluid inclusion, in which 63 other elements were recorded at the same time (LECO Renaissance with LA-system of Fig. 2). Resulting intensity ratios (relative standard deviation, RSD, 1σ) are more reproducible than with quadrupole instruments, provided that count rates are sufficiently high.

surement of instrument background for all elements. The limit of detection (LOD) for each element can be calculated from the minimum detectable signal intensity, defined by 3 times (for >99% confidence) the standard deviation of the background measurement. If the durations of background and signal acquisitions are similar, the LOD is given by insertion of the minimum detectable signal intensity into Eqn. 1:

$$\mathrm{LOD} = C_r^{\mathrm{SAMP}} \cdot \frac{C_i^{\mathrm{STD}}}{C_r^{\mathrm{STD}}} \cdot \frac{3\ \sigma_i^{\mathrm{BG}}\ I_r^{\mathrm{STD}}}{I_r^{\mathrm{SAMP}}\ I_i^{\mathrm{STD}}} \qquad (2)$$

or the corresponding formula in Longerich et al. (1996b) for the general case.

3.2. Verification of Matrix-Insensitive Calibration for Homogeneous Solids

The practicality of internal standardisation builds on the great ability of LA-ICPMS to measure from major (tens of wt.%) down to trace (ng/g) element concentrations in a single microscopic sample volume. This permits the combination of trace-element analysis by LA-ICPMS with independent determination of major-element concentrations by electron microprobe (EMP) or from assumptions based also on crystal stoichiometry. The applicability of LA-ICPMS equally depends on the availability of reliable external calibration standards. Extensive tests have shown that, with the laser-optical system used here, external calibration is surprisingly matrix-insensitive and linear over the entire concentration range. Reproducible and accurate results were obtained by comparison between synthetic and natural glasses using different analytical techniques including EMP and SIMS (Horn et al., 1997; Sylvester and Eggins, 1997). With the ablation system of Figure 2, accurate cross-calibration has been demonstrated between very different matrices, including synthetic silicate glass standards from NIST, aqueous fluid samples ablated through the walls of thin plastic tubes (Günther et al., 1997b), other glasses with different metal ratios (Mank and Mason, 1999), natural basalt glass (Fig. 7a), $Li_2B_4O_7$ flux pellets of bulk silicate rocks (Odegard and Hamester, 1997; Günther et al., 2001b; Sylvester, 2001b; Fig. 7b) and rock-forming silicate and oxide minerals (Figs. 7c and 7d). The grey bar in Figure 7d shows that all major elements (oxide concentrations > 10 wt.%) in clinopyroxene, amphibole and spinel, analysed by LA-ICPMS in one run with additional eight trace-elements, agree within 4% or better with the respective EMP analyses. These and numerous other tests illustrate that any element in any oxygen-rich (oxide, borate, silicate, carbonate, etc.) matrix can be used as internal standard or analyte and calibrated using NIST glasses. For sulfides, external standardization was successfully carried out with sulfide standards (Sylvester, 2001c), and recent tests indicate that the ETH/GeoLas system even allows accurate cross-calibration between Cu-Fe-(-Ni-Co) sulfides and silicate glasses (Halter et al., 2002b, 2003).

3.3. Depth-Profiling Without Fractionation

UV laser systems with ideal flat-top beam profiles (Fig. 2) remove sample material at a rate of ~0.1 μm per shot. In principle, this allows compositional depth profiling, as tested with variable success by Kanicky et al. (1997), Simon et al. (1997), Mank and Mason (1999), Bleiner et al. (2000b), and Plotnikov et al. (2001). Minimal time-dependent fractionation in homogeneous samples (Figs. 3a and 4) and the accuracy of comparative tests across different matrices (Fig. 7) indicate that representative compositional data are acquired throughout the progress of ablation with the GeoLas imaging system (Mason and Mank, 2001). Figure 8 shows the results of progressive ablation into a natural crystal face exhibiting optical zonation at the micron scale in cross-section. The high-resolution compositional profile obtained by ablation into the cassiterite surface is in agreement with the low spatial resolution data obtained on a cross-section through the same crystal surface, even for Nb which varies by 2 orders of magnitude in concentration. With

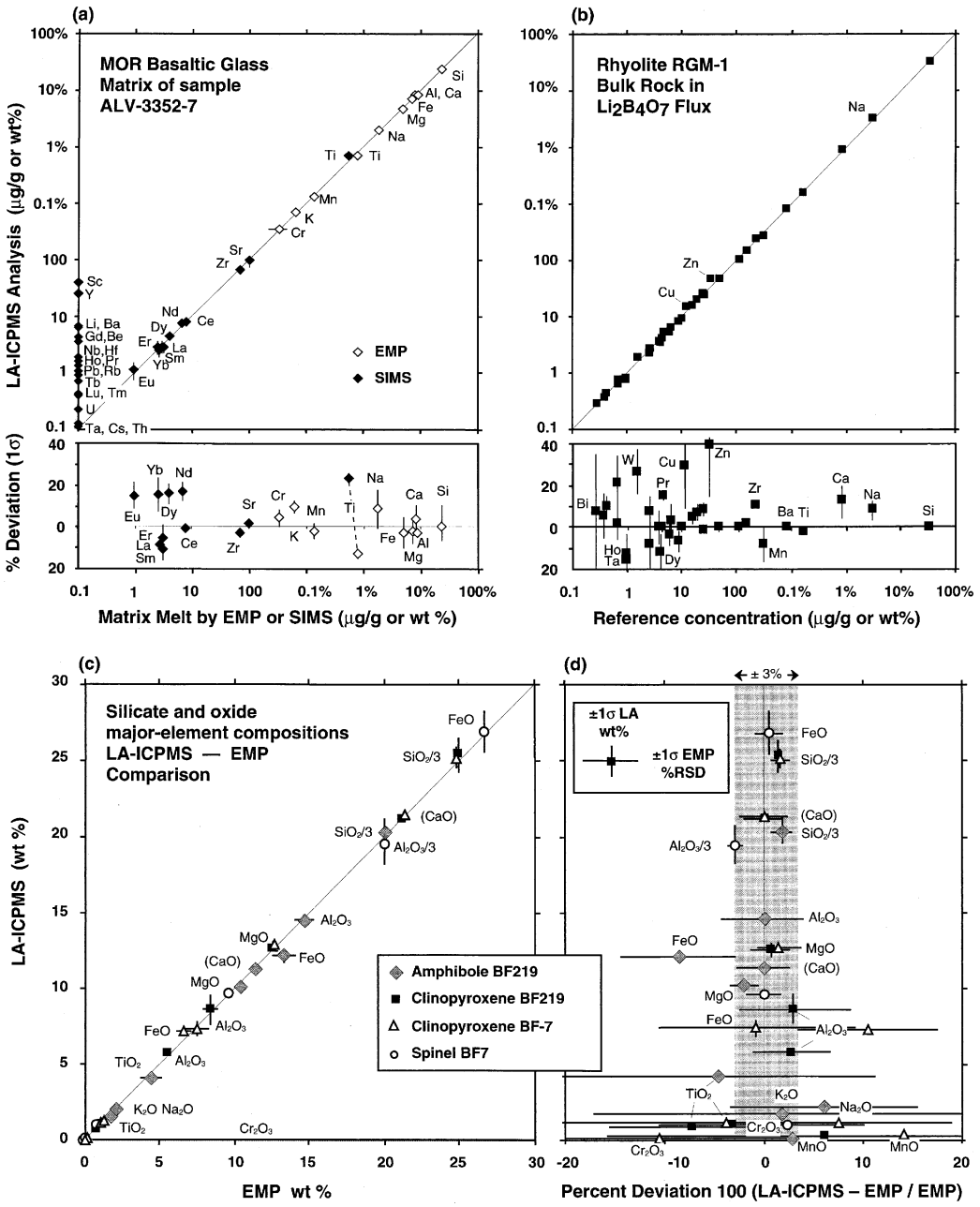

Fig. 7. Accuracy-tests showing the validty of matrix-insensitive external calibration of LA-ICPMS analysis of homogeneous materials by a common silicate glass standard (SRM610 from NIST), across a large concentration range from tens of wt.% to sub-μg/g concentrations in a single analytical run. LA-ICPMS analyses on the vertical axis are plotted against certified values or analyses by independent methods on the horizontal axis. (a) Matrix glass of a fresh basalt from the southern East Pacific Rise (17°–19°S; sample ALV-3352-7, STOWA cruise; Sinton, 1999). SIMS analyses performed at the Woods Hole Oceanographic Institution (WHOI) using a Cameca IMS 3f ion probe at 4.5 kV (Shimizu and Hart, 1982), standardized with basalt glass KL-2 and reduced relative to ^{28}Si. Spot size was 10 μm using an offset of –90 V to reduce molecular ion interferences. Trace-elements by SIMS (~1–100 μg/g) and major elements by EMP (~0.1–50 wt.%) are in good agreement with LA-ICPMS results obtained from a 40-μm crater with a single 40-element menu that included an additional 19 trace elements marked on the left vertical axis. Deviations (±3% RSD on average) shown below the main diagram. (b) Whole-rock analysis by LA-ICPMS of $Li_2B_4O_7$ flux pellets, using Li as internal standard (25 wt.% RGM-1 Rhyolite plus 75 wt.% $Li_2B_4O_7$; Günther et al., 2001b). (c) Amphibole, clinopyroxene and spinel from two samples from the Braccia gabbro complex (Northern Italy), comparing LA-ICPMS data for all major elements with EMP data on the same minerals (Hermann et al., 2001). (d) Deviations for the data set of (c), with error bars marking the reproducibilities for the two analytical methods (the deviation of FeO for amphibole is attributed to the inclusion of dusty cores in the EMP average, whereas only clear rims were measured by LA-ICPMS).

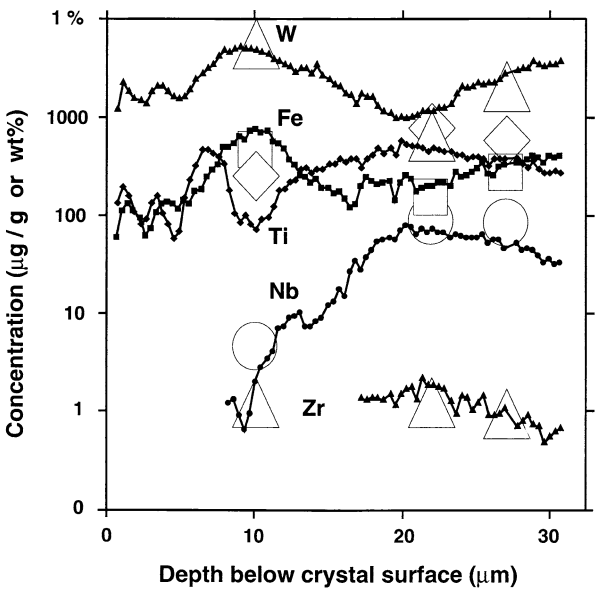

Fig. 8. Depth profiling perpendicular to the growth surface of a cassiterite crystal. Data from stepwise ablation with an 80-μm crater at an average resolution of 0.37 μm (integrating three shots separated by a pause, for each small symbol) is compared with spot analyses from individual 6-μm craters in an exposed cross-section of the same crystal edge (large faint symbols). The agreement of the low- and high spatial resolution results shows that element fractionation at the ablation surface is insignificant at least down to crater depths of half the crater diameter in this instance (sample VIL2 from Viloco, Bolivia).

single laser shots, LA-ICPMS allows quantitative compositional depth-profiling at a resolution of $\sim$0.1 μm, subject to sample removal occurring dominantly from the floor of a large shallow ablation pit. Such measurements bridge the depth-resolution range between surface profiling by SIMS (atomic scale to nm; Gerson et al., 1999; Zalm, 2000) and the spot size of EMP or trace-element 'microprobes' on an exposed sample surface ($>$1–10 μm), and has promising applications in studies of diffusion and reaction processes (e.g., Ghazi et al., 2002).

4. QUANTITATIVE ANALYSIS OF FLUID AND MELT INCLUSIONS

Controlled and representative ablation without selective loss of material, as demonstrated for solid analytes in the preceding sections, is the key prerequisite for quantitative microanalysis of multiphase melt and fluid inclusions. Following representative sampling of the entire inclusion, quantification of an inclusion signal requires a procedure comprising signal integration, subtraction of host-mineral contributions, and calibration of element ratios using an external standard (Eqn. 1). For the calculation of element concentrations, the ICPMS results are combined with an internal standard on the absolute concentration scale. This may be an independently measured or inferred element concentration in the case of melt inclusions (Halter et al., 2002a), or a microthermometric measurement that can be related to experimentally known *T-X* phase relations for fluid inclusions.

4.1. Representative Sampling of Heterogeneous Inclusions

Geochemically meaningful fluid and melt inclusions are trapped as a single phase at high temperature and pressure, which upon cooling to room temperature usually separates into a heterogeneous phase mixture. Most fluid inclusions split into gas, liquid and precipitating crystals. Even apparently simple aqueous inclusions may contain a major proportion of a particular trace element adsorbed to the inside wall, or as a daughter crystal that is too small for visual detection. Silicate melt inclusions may crystallize and exsolve volatile-rich phases unless quenching is very rapid (i.e., glassy melt inclusions). They always precipitate a rim of host mineral upon cooling, thereby fractionating some components that were part of the homogeneous melt at the time of entrapment. Sulfide melts cannot be quenched even under laboratory conditions. The main challenge of melt and fluid inclusion analysis is therefore the reconstitution of heterogeneous microsamples, to obtain the composition of the original fluid or melt phase.

Extensive testing has shown that for fluid inclusions, representative laser sampling is best achieved by first 'drilling' a small hole into an inclusion to release any gas and a part of the aqueous phase, and subsequently widening the crater to ablate the remainder of the aqueous liquid and all solid internal precipitates (Günther et al., 1998). The time-resolved LA-ICPMS signal from the ablation of a polyphase fluid inclusion yields variable intensity ratios throughout the ablation process, and this time variation provides useful qualitative information about the composition of the multiple phases present at room temperature, as illustrated by Figure 9. For quantification of the bulk fluid composition, intensities must be integrated over the entire interval of inclusion ablation. The tests described below demonstrate that even very complex signals, such as that shown by Figure 9b, are by no means erratic but lead to reproducible and accurate bulk compositions of heterogeneous fluid and melt inclusions.

4.2. Calibration for Absolute Element Concentrations in Fluid Inclusions

For water-rich fluid inclusions, we have tested a calibration procedure using Na as internal standard, because this element dominates in most natural fluids and the apparent salinity of NaCl-rich fluid inclusions can be determined by microthermometry. At present, this seems to be the only practical approach to quantitative concentration analysis for fluid inclusions (Fig. 10) and is therefore described in detail.

After petrographic characterization and interpretation of inclusion assemblages (Goldstein and Reynolds, 1994), the first step of quantitative analysis of an aqueous fluid inclusion is the microthermometric determination of the apparent salinity (NaCl equivalent wt.%), based on the temperature of final dissolution of solids (ice, hydrohalite, clathrate or halite) and experimental phase equilibria in the NaCl–H_2O (–CO_2) model systems (Bodnar and Vityk, 1994; Diamond, 1994). During the following LA-ICPMS run, one or several external standards are measured twice each, then up to 16 microthermometrically characterized fluid inclusions are ablated using the stepwise opening procedure illustrated in Figure 9. Finally each standard is measured twice again to correct for any drift in instrument sensitivities. If an inclusion is not too shallow, the overlying

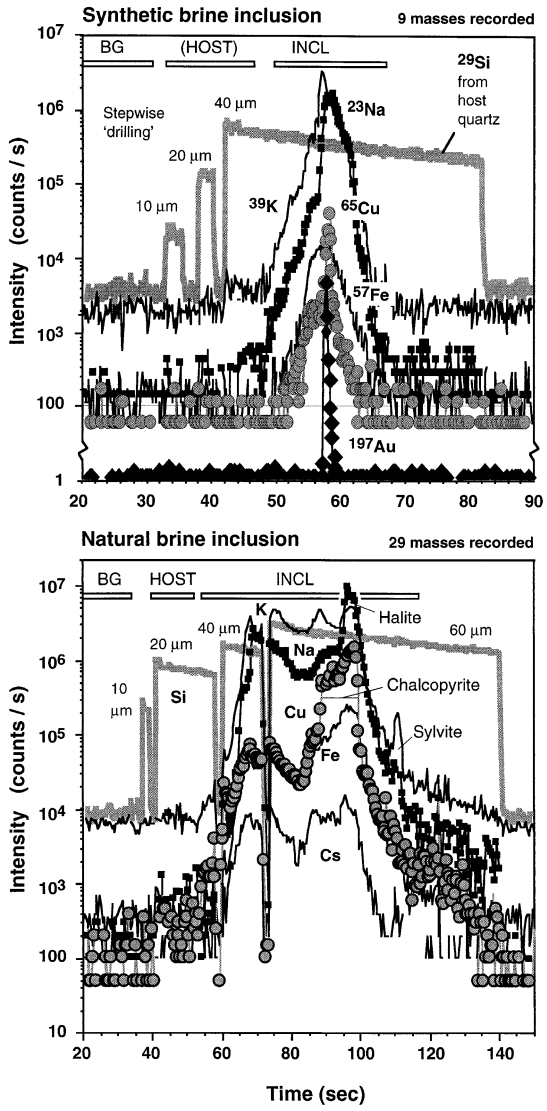

Fig. 9. Transient signals recording typical ablations for representative sampling of polyphase fluid inclusions, using a stepwise increase of beam diameter at constant surface intensity on the sample. The signals show the mass spectrometer response for selected masses as the ablation proceeds through several steps, starting with a 10-μm hole and ending with the complete removal of the entire inclusion and the immediately surrounding host in a 40- to 60-μm crater, as shown by the Si signal monitoring the ablation of the host quartz. Short drops in ^{29}Si intensity between the 10-, 20-, 40- and 60-μm peaks are due to blanking of the laser beam during aperture switching. (a) Signal from a synthetic brine inclusion, where parallel signals of K, Fe and most of the Cu represent liberation of the aqueous solution from the inclusion; superimposed is the ablation of a halite daughter crystal (sharp rise of Na at 58 s), and a small Cu-rich opaque crystal containing all of the detectable gold (sharp coincident Cu and Au signals at 59 s). With only six elements recorded in this run, even brief transient signals are well defined by sequential quadrupole mass-spectrometry, leading to an excellent reproducibility among a single population of similar inclusions in this sample ($\pm$5% RSD for all integrated element ratios, including Au/Cu). (b) A typical signal from a large natural brine inclusion (45-μm diameter), emptied during the last three steps of ablation with successive 10-, 20-, 40- and 60-μm crater diameters, recording 29 elements sequentially during each mass sweep. The larger number of recorded elements reduces signal definition, leading to lower reproducibilities of integrated intensity ratios and absolute element concentrations (typically $\pm$20%; see Fig. 13).

sample surface is preablated with a few large-diameter low-energy cleaning shots. SRM610 from NIST is routinely used as the external standard for most major and trace-elements. Solid halite (for Cl) or polyethylene capillaries filled with a standard solution and welded shut with a fine soldering iron (Günther et al., 1997b) are successfully used as additional standards for elements unavailable in standard silicate glasses at appropriate concentrations (Fig. 3b). Cross-calibrations between these different standard materials showed no significant differences in sensitivity ratios, confirming that matrix matching between standard and sample is not required with our optical system.

After the analytical session, the complex ablation signal from each inclusion is inspected, to set three time intervals (Fig. 9). The first interval measures instrument background before ablation (BG). The second interval represents a period of pure host-mineral ablation (HOST) before breaching of the inclusion (for shallow inclusions, the HOST signal can be obtained with a separate host ablation nearby). A third time interval (INCL) encompasses the first sharp rise of Na and other elements, as the inclusion is first pierced, through to the decay of the inclusion signal back to host-mineral background. Total count rates in each interval are integrated, and the average instrument background (BG) is subtracted from the following two intervals. Thus, background-corrected average intensities for each element, including Na and Si, are obtained. The signal from the inclusion ablation is a function of the inclusion contents plus variable contributions from the host mineral. Even in quartz these can be significant (e.g., for Li, Na, Al, Sb, Sn) but are readily subtracted by assuming that the Si signal monitors the contribution of quartz host only and is not significantly present in the fluid. Host-mineral corrected intensities, representing the contribution from the fluid inclusion alone, are then given by

$$I_i^{\mathrm{INCL}} = I_i^{\mathrm{MIX}} - I_{\mathrm{Si}}^{\mathrm{MIX}} \cdot \frac{I_i^{\mathrm{HOST}}}{I_{Si}^{\mathrm{HOST}}}. \quad (3)$$

In the more general case where all elements are present to different degrees in both the host and the inclusion, an iterative calculation is required to deconvolve the signal contributions and to determine the composition of the inclusion alone (Halter et al., 2002a).

Using Eqn. 1, which relates the integrated net signal intensities from the fluid inclusion to those of the external standard and its element concentration ratios, we obtain the concentration ratio of elements in the inclusion. These are expressed relative to the internal standard, chosen to be Na:

$$\frac{C_i^{\mathrm{INCL}}}{C_{\mathrm{Na}}^{\mathrm{INCL}}} = \frac{C_i^{\mathrm{STD}}}{C_{\mathrm{Na}}^{\mathrm{STD}}} \cdot \frac{I_i^{\mathrm{INCL}}\, I_{\mathrm{Na}}^{\mathrm{STD}}}{I_{\mathrm{Na}}^{\mathrm{INCL}}\, I_i^{\mathrm{STD}}}. \quad (4)$$

The next step is to combine the element ratios from the ICPMS with the microthermometric NaCl equivalent wt.% concentrations to calculate absolute element concentrations. This requires knowledge of the effect of dissolved components other than NaCl upon the melting temperatures of ice, hydrohalite, clathrate or halite. The empirical formula

$$\text{NaCl equivalent wt.\%} = C_{\mathrm{NaCl}} + 0.5 \cdot [C_{\mathrm{KCl}} + C_{\mathrm{FeCl_2}} + C_{\mathrm{CaCl_2}} + \ldots] \quad (5)$$

is based on the experimental observation that halide solubility

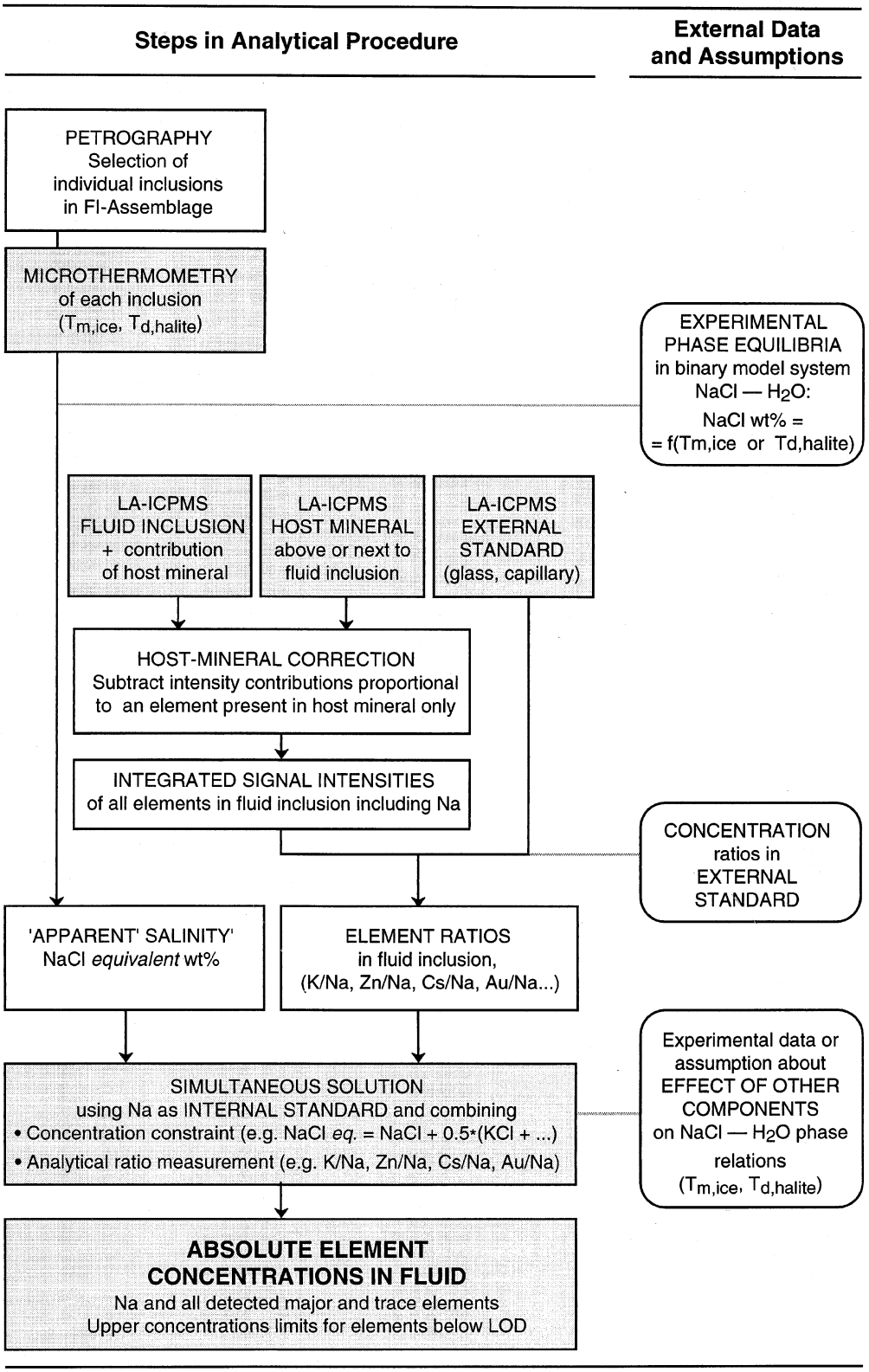

Fig. 10. Flow diagram for the quantification of element concentrations in natural fluid or melt inclusions, based on the combination of LA-ICPMS measurement with independent information about an external standard (e.g., NIST glass) and an internal standard (e.g., Na from microthermometry). See text for explanation.

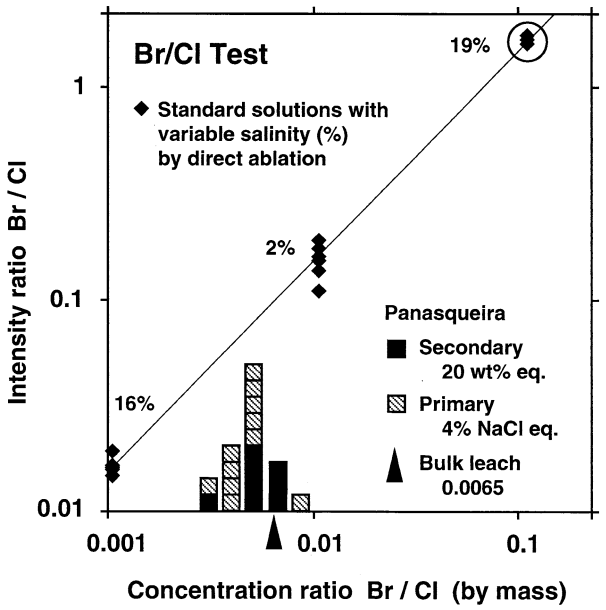

Fig. 11. Calibration plots for optimized analysis of Cl/Br ratios in three standard solutions and two generations of fluid inclusion in a quartz sample of the Panasqueira W-Sn deposit. Direct liquid ablation of the standard solutions of variable salinity and Br/Cl ratio, enclosed in polyethylene capillaries, was used for external calibration (Günther et al., 1997b; last signal in Fig. 3b). ICPMS data acquisition was optimized for small single-inclusion signals, by alternate counting for 5 ms on ^{35}Cl and 25 ms on ^{79}Br only. Small low-salinity primary inclusions (4 wt.% NaCl equivalent) in the Panasqueira sample have an average Br/Cl ratio of 0.0048 ± 0.0014 (1σ), which is marginally lower than that of large higher-salinity secondary inclusions (20 wt.% NaCl equivalent; Br/Cl = 0.0063 ± 0.0031). The secondary inclusions volumetrically dominate in the sample, and their Br/Cl analyses by LA-ICPMS results are in agreement with three precise bulk leachate analyses (0.0066, 0.0066, 0.0064) obtained by D. Banks (Noronha et al., 2001, and written communication) on aliquots of the same sample.

and ice-melting isotherms depart at approximately right angles from the NaCl-H_2O join in ternary phase diagrams with KCl, $CaCl_2$ and $FeCl_2$ (Heinrich et al., 1992). Simultaneous solution of Eqn. 4 and 5 permits evaluation of absolute concentrations of all major and trace element concentrations in the fluid.

In practice, those cations M having reproducible M/Na > 0.1 in an inclusion assemblage are included in the empirical formula (i.e., M = K, Fe and Mn in typical magmatic fluids; Ca usually shows great scatter, unless measured by dynamic reaction cell). Using Cl instead of Na as internal standard will lead to identical results, if Eqn. 5 is applied to a perfectly charge-balanced analysis involving only chloride salts. Cl signals in multi-element analyses of fluid inclusions are weaker and often close to the detection limit (Günther and Heinrich, 1999a), such that the uncertainties of all results will generally be greater than with the use of Na as internal standard. Nevertheless, Cl and also Br can be measured with a reduced element menu and lead to consistent Br/Cl ratios, as shown in Figure 11 by a calibration test and an application to halite-undersaturated fluid inclusions.

4.3. Limits of Detection and Uncertainties

The limit of detection (LOD) is evaluated on the basis of the standard deviation of the instrument background signals (Longerich et al., 1996), for each element in every inclusion. Where inclusion intensities after background-subtraction and host-mineral correction fall below this significance limit, a maximum likely concentration of the element is calculated by applying the full evaluation procedure (Eqn. 1–5, Fig. 10) to the minimum significant intensity, $3\sigma_{BG}$. Sometimes, a small peak of an element can be clearly recognized as detected, because of its consistent association with the short peak of other elements present in the daughter crystals of an inclusion assemblage (e.g., Au in Fig. 9a). In such cases, the statistical significance limit may be relaxed to $2\sigma_{BG}$ or $1\sigma_{BG}$ to obtain a semiquantitative concentration estimate.

Detection limits in fluid inclusions are strongly element-dependent, due to mass-dependent instrument sensitivity and variable abundance of the chosen isotope. They are also a complex function of inclusion size and shape, signal shape and duration, and the number of elements to be recorded from a single inclusion (Fig. 12). Typical detection limits achieved for most heavy elements (above mass ~100) in a multi-element menu (20–40 isotopes) are ~1 μg/g in a near-spherical 25-μm brine inclusion. For a given inclusion mass and ablation time, detection limits and signal definition can be improved if fewer elements are recorded more frequently and during correspondingly greater total integration times. With some instruments, dwell times can be set individually for each element in the measurement cycle. Thus, detection limits as low as 0.1 μg/g Au were obtained with a short 100-ms cycle, which included 10-ms dwell times on Si, Cu, As and Na and a 50-ms dwell time on Au, yielding an effective counting efficiency near 50% on ^{197}Au (Ulrich et al., 1999). With decreasing inclusion size, limits of detection deteriorate approximately with inclusion volume (i.e., with the third power of inclusion diameter), but inclusions larger than ~25 μm diameter do not yield a corresponding improvement because of the typically extended duration of complete ablation (Günther et al., 1998).

A rigorous calculation of uncertainties in a single fluid-inclusion analysis is difficult because of the large number of experimental variables and the critical influence of signal shape. A clearer definition of uncertainty and its sources is gained by comparing the results from an assemblage of inclusions with presumably uniform composition. The twelve inclusions shown in Figure 13 were all located on a single healed fracture at 5 to 50 μm mean depth below the surface of a quartz plate. The inclusions have similar petrographic (subequant shapes, same phase proportions including several daughter crystals) and microthermometric properties (54–63 NaCl equivalent wt.% determined from halite dissolution), but their size varies between 7 and 26 μm average diameter. This dataset exemplifies the analytically most difficult case of complex polyphase brine inclusions with halite, sulfide and oxide daughter crystals (Ulrich et al., 2001). The uncertainty contributed by the counting statistics of the integrated background and signal intensities alone are readily evaluated, and indicated in Figure 13a by error bars ($\pm 1\sigma$) where they exceed the symbol size. Figure 13a shows that counting statistics is the dominant contribution to uncertainty for elements close to the detection limit, such as Li, Bi and U in this example. For these elements, where individual results overlap within widely variable uncertainties, the calculation of error-weighted means within an assemblage of cogenetic inclusions can be appropriate. For elements well

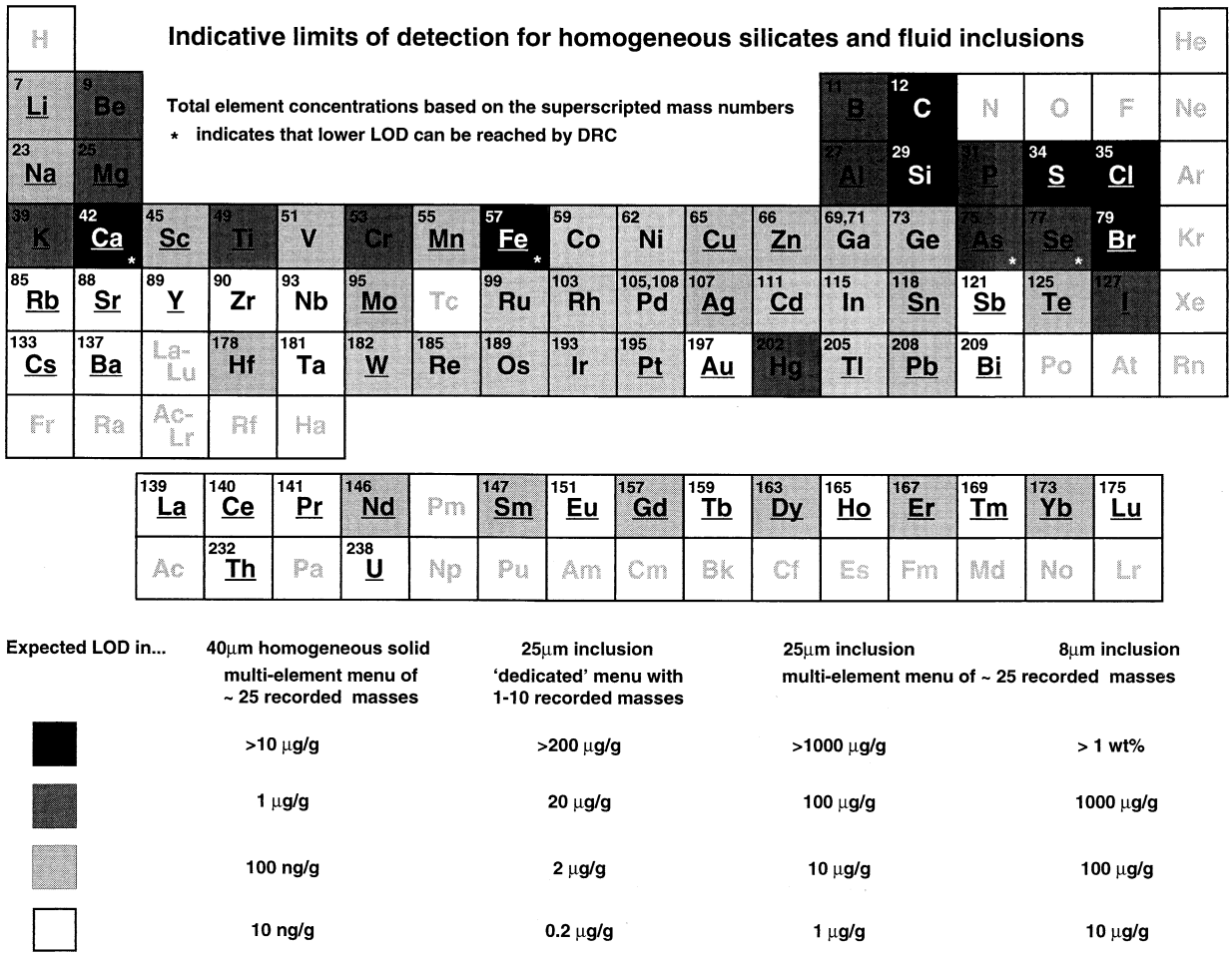

Fig. 12. Periodic table of the elements giving an order-of-magnitude indication of typically achieved or expected limits of detection for LA-ICPMS analysis of solids, and of fluid or melt inclusions as a function of inclusion size and the number of elements measured simultaneously. Underlined elements were actually measured at the indicated concentration levels in natural or synthetic fluid inclusions hosted by quartz. For other elements the expected limits of detection are inferred from measurements on homogeneous solids. Numbers at the upper left of each element symbol indicate the mass typically used for fluid inclusion analysis, an asterisk in the bottom right corner indicates that limits of detection may be significantly improved by measuring a different mass using a dynamic reaction cell. Indicated concentration limits are for optimal cases, and may be significantly poorer depending on matrix composition (polyatomic interferences), host mineral composition (deconvolution of inclusion and host contributions), and inclusion geometry (shape, depth, daughter crystals) which affect the transient signal shape.

above their detection limit, however, counting uncertainties are within the symbol size of Figure 13a, yet inclusion-to-inclusion variability is much larger and probably gives a more realistic measure of analytical uncertainty. Absolute concentrations based on Na as internal standard typically vary by ±20%, but ratios between elements that occur dominantly in the aqueous phase are more constant (±10–15% for ratios among Mn, Zn, Rb, Ba in this case). In Figure 13a, the calculated concentrations of these elements show a distinct covariation that is inversely correlated with that of Na. This indicates that the overall analytical precision in this inclusion assemblage is probably still limited by the quality of laser ablation, and that imperfect sampling of the halite daughter crystal (containing about half of the Na present in these inclusions) and resulting signal fluctuations are probably the dominant source of scatter. Similarly, imperfect sampling of small chalcopyrite daughter crystals is responsible for the relatively large scatter of Cu concentrations. Inclusion #4 is an extreme outlier in Cu, probably because the entire chalcopyrite daughter crystal was lost during ablation.

Figure 13a shows how reproducible results of geochemically useful precision are obtained by internal standardization using microthermometric apparent salinity and LA-ICPMS intensity ratios. By contrast, absolute signal intensities vary over > 2 orders of magnitude between individual co-genetic inclusions, due to variations in size, depth, internal phase geometry and ablation duration. It is evident from this test that neither absolute (Fig. 13b) nor volume-normalized (Fig. 13c) intensities have any direct relation to absolute element concentrations. Attempts at calibration without an internal standard will generally not provide even the right order of magnitude for absolute element concentrations. Absolute calibration procedures as

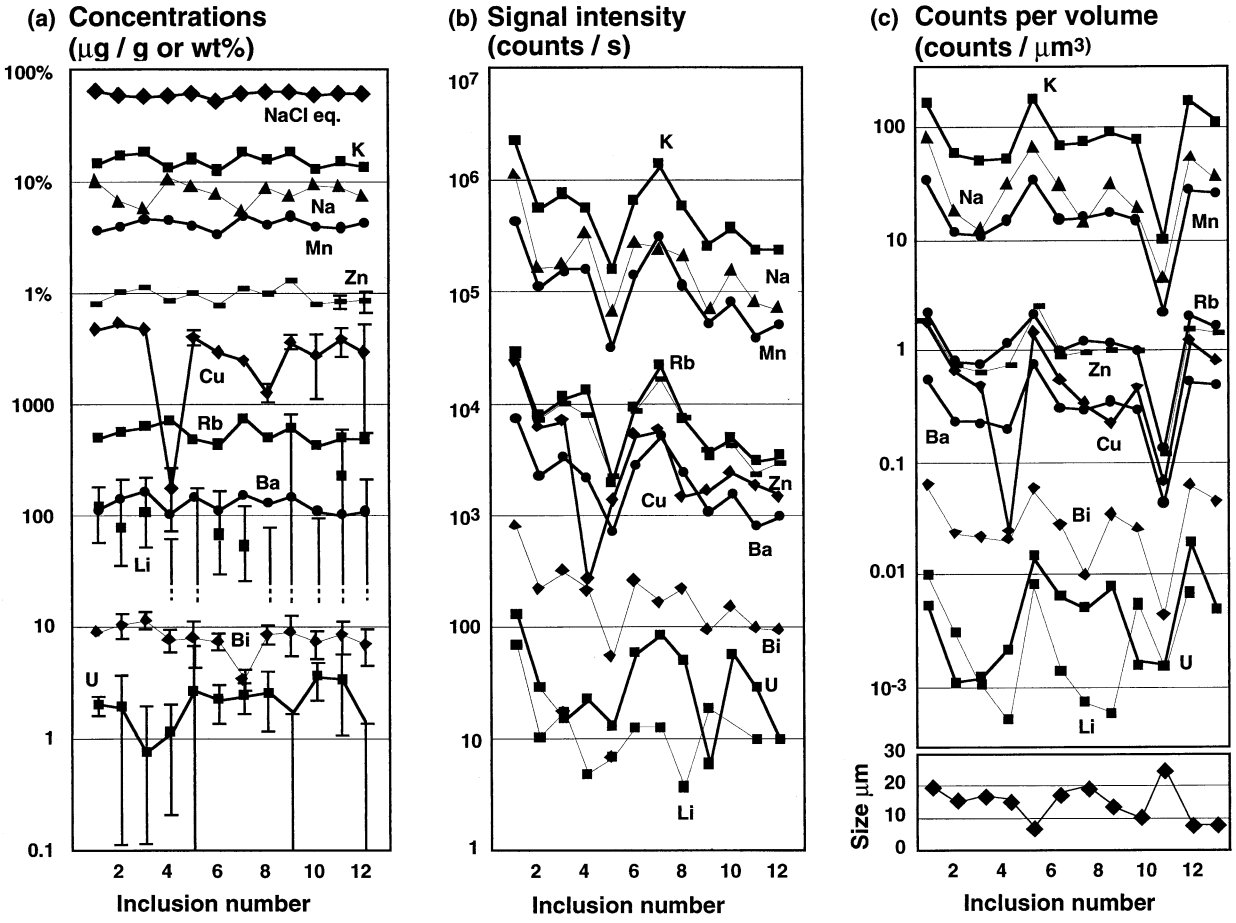

Fig. 13. Assessment of analytical precision for natural fluid inclusions, using LA-ICPMS analyses from an assemblage of 12 petrographically similar brine inclusions along one healed microfracture in quartz (Bajo de la Alumbrera porphyry-copper deposit; Ulrich et al., 2001). A representative selection of 10 elements from a full menu of 25 are plotted to illustrate reproducibility and sources of uncertainty. (a) Element concentrations obtained by external standardization with SRM610 glass and internal standardization using Na (corrected NaCl equivalent wt.% from microthermometry, Fig. 10 and Eqn. 5). The total uncertainty from counting statistics is indicated by error bars, where it exceeds symbol size. For elements below detection, calculated upper concentration limits are shown by bars extending towards the bottom of the diagram. (b, c) Absolute signal intensity (b; in counts per s) and total counts normalized to inclusion volume (c; in counts per μm^3) vary over 2 orders of magnitude, demonstrating that absolute element concentrations cannot be obtained without an internal standard.

proposed by Ghazi and Shuttleworth (1999) are, at best, applicable to the analysis of the aqueous phase of large flat inclusions immediately below a sample surface.

4.4. Accuracy Tests Using Synthetic Fluid Inclusions

The accuracy of our quantification procedure has been extensively tested by cross-calibrations between silicate glasses, direct ablation of aqueous standard solutions in plastic capillaries and synthetic fluid inclusions of known composition in quartz (Günther et al., 1997b, 1998). Matrix dependencies among the widely variable standard materials are insignificant compared with the typical variability of results from complex natural inclusion assemblages. As a test of the LA-ICPMS analysis procedure, we analysed a number of synthetic aqueous inclusions in a sample previously analysed by micro-PIXE (Ryan et al., 1995). The results (Fig. 14) allow a three-way comparison that indicates excellent consistency between the prepared fluid composition, our LA-ICPMS analyses and the micro-PIXE analyses on the same sample. Inclusion-to-inclusion scatter of micro-PIXE is slightly smaller than that of LA-ICPMS (both indicated by 1σ error bars), notably for Zn which is present in a small daughter crystal in some of the inclusions. The results include accurate data also for Cl in inclusions with a total salinity of 23 wt.%, even though Cl signals are weak. In most natural fluid samples that we analysed for Cl, there is a tendency towards an anion deficit when looking at the averages in a fluid inclusion assemblage (Audétat et al., 2000a; Ulrich et al., 2001). This could suggest the presence of other anions such as F, but can be more simply explained by a bias towards positive averages due to the omission of numerous Cl analyses below the limit of detection.

Systematic errors in LA-ICPMS analysis of fluid inclusions

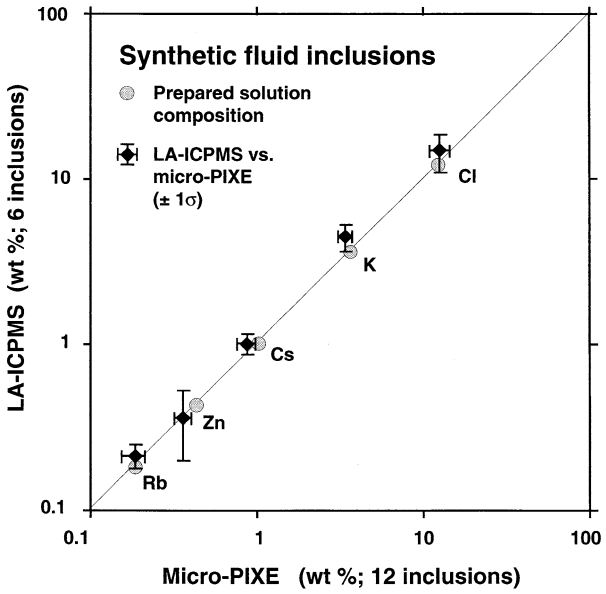

Fig. 14. Concentrations of selected elements in synthetic fluid inclusions in quartz analysed by LA-ICPMS, plotted against micro-PIXE analyses for the same sample (Ryan et al., 1995). Both microanalytical methods agree with the prepared fluid concentrations, shown by small open circles. SRM610 (for Na, K, Zn, Rb and Cs) and pure halite (for Cl) were used as external ICPMS standards, and all data were calculated on the basis of the prepared Na concentration (5.36 wt.%). Error bars denote 1σ variablity among the indicated number of inclusions, which ranged in size from 10 to 60 μm.

can arise from simplifying assumptions about the internal standard. The possible magnitude of these errors can be judged from a number of experiments summarized in Table 1. The simple Eqn. 5, relating concentrations in a complex salt mixture to that of Na and the NaCl equivalent wt.% value, introduces an error which is likely to increase with the deviation of the inclusion composition from the binary H_2O-NaCl system. Table 1 indicates that for typical NaCl-dominated crustal fluids this error is unlikely to be a major problem. In most cases, the uncertainty will have a similar magnitude ($\sim$20%) as the typical laser sampling uncertainty indicated by the reproducibility in one inclusion assemblage. For fluids containing high concentrations of salts in excess of NaCl, however, the error may increase up to 50% (or more in the case of major concentrations of Li). On the other hand, the data in Table 1 also demonstrate that the empirical correction (Eqn. 5) leads to an essential improvement in accuracy compared to complete neglection of components other than NaCl.

Less tractable ambiguities are caused by major elements that partly reside in a daughter crystal, at the temperature of the phase transition used for the calculation of apparent salinity. For example, the Fe present as insoluble hematite at the temperature of final dissolution of halite should not be included in the correction formula (Eqn. 5), yet the proportions of Fe in hematite and in aqueous solution can at best be estimated approximately from the signal shape. In weakly CO_2-bearing aqueous fluids of low salinity, whose salt concentration is difficult to assess from microthermometric data (Diamond, 1994), only cation ratios and upper concentration limits may be obtainable. No possibility exists at this point to calibrate absolute concentrations of metals in vapor-rich inclusions containing no visible aqueous phase at room temperature. Therefore, Ulrich et al. (2001) had to resort to vapor-phase salinities estimated from experimental phase diagrams for the NaCl-H_2O solvus and the measured salinity of coexisting brine inclusions, which effectively leads to estimates of minimum metal concentrations.

4.5. Silicate Melt Inclusions

LA-ICPMS has been used for trace-element analysis of exposed glassy melt inclusions (e.g., Taylor et al., 1997; Span-

Table 1. Microthermometric tests of the empirical correction (Eqn. 5) for the effect of other components on NaCl equivalent wt.%.

Sample	Method	Composition (wt. ratios of elements, al added as chlorides)	NaCl true	$T_{m,ice}$ ($T_{m,halite}$*)	NaCl eq. wt.%	NaCl corr	Uncorr/ true	Corr/ true
AA-23/3/00	Synflinc	Na : K : Fe = 1.0 : 0.6 : 0.5	34.4	440*	52.0	35.4	1.5	1.0
RF-14/11/96	Synflinc	Na : K = 1.0 : 0.3	20.0	–19.8	22.2	19.9	1.1	1.0
PO-1	Paraffin oil	Na : Ba = 1.0 : 8.2	3.1	–7.1	10.7	3.1	3.5	1.0
PO-2	Paraffin oil	Na : Ba = 1.0 : 1.7	10.0	–11.6	15.8	10.5	1.6	1.1
PO-3	Paraffin oil	Na : K : Ba = 1.0 : 2.8 : 1.4	4.3	–8.2	12.1	4.9	2.8	1.1
AA-23/6/01-R	Synflinc	Na : K : Mn : Fe = 1.0 : 1.0 : 1.0 : 1.0	3.0	–6.2	9.5	4.2	3.2	1.4
AA-23/6/01-L	Synflinc	Na : K : Mn : Fe = 1.0 : 1.5 : 1.5 : 1.5	3.0	–8.5	12.3	4.2	4.1	1.4
AA-28/6/01-L	Synflinc	Na : K : Mn : Fe = 1.0 : 1.0 : 1.3 : 1.0	7.4	–24.2	25.1	10.5	3.4	1.4
AA-28/6/01-R	Synflinc	Na : K : Mn : Fe = 1.0 : 1.6 : 1.3 : 1.3	7.0	–31	29.3	10.5	4.2	1.5
PO-4	Paraffin oil	Na : Li = 1.0 : 0.85	5.8	–24.1	26.2	13.0	4.5	2.2
PO-5	Paraffin oil	Na : Li = 1.0 : 4.6	1.6	–33.8	33.5	5.2	20.8	3.2

NaCl true = actual NaCl concentration in prepared mixture; $T_{m,ice}$, $T_{m,halite}$ = temperature of last melting of ice or halite; NaCl eq. wt.% = apparent salinity from microthermometry and equilibria in NaCl-H_2O system (Bodnar and Vityk, 1994).

NaCl corr = corrected NaCl concentration using Eqn. 5; Uncorr/true = NaCl eq. wt.%/prepared NaCl concentration; Corr/true = corrected NaCl concentration/prepared NaCl concentration.

* Microthermometric measurements of last melting of ice ($T_{m,ice}$) and halite ($T_{m,halite}$) in synthetic fluid inclusions (synflinc) or microscopic solution droplets prepared as an emulsion in paraffin oil. Most of the prepared compositions represent extreme deviations from common NaCl − H_2O dominated natural fluids. Even for these, the deviations after empirical correction using Eqn. 5, as shown in the last column of the table, are much smaller than if no correction was applied. Assuming $BaCl_2$ as a proxy for other divalent chloride salts, the first five experiments encompass the range of most complex natural brines, indicating that systematic errors after correction are generally <20%.

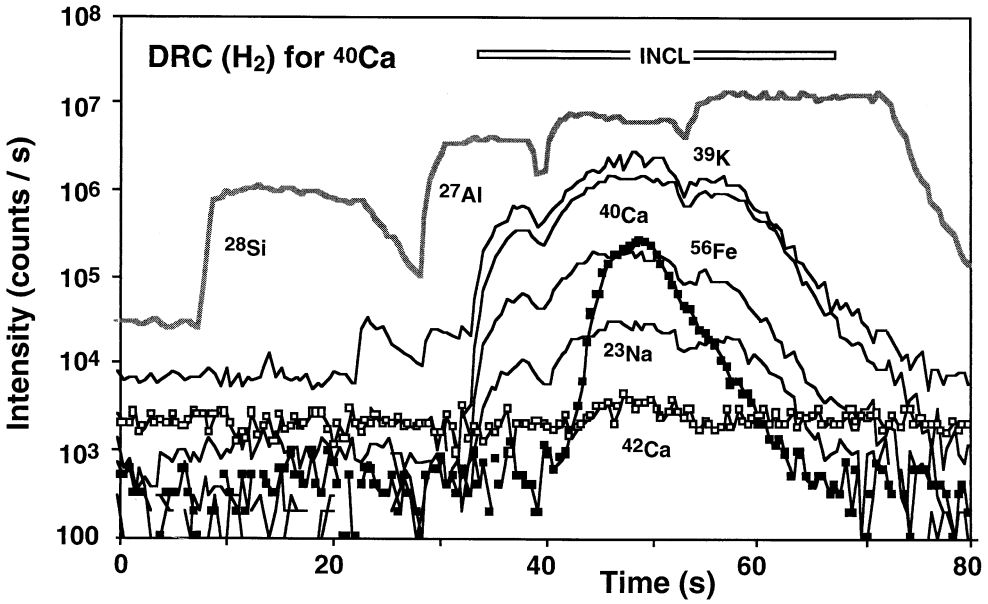

Fig. 15. Transient signal of ablation of a small Ca-poor silicate melt inclusion from the Mole Granite (Australia), recorded with a dynamic reaction cell ICPMS (Perkin Elmer–SCIEX Elan 6100DRC) using Ne as buffer gas and H_2 as reaction gas. Note the low background of mass 40, which in normal quadrupole mode is occupied by $\sim 1 \times 10^9$ counts/s due to $^{40}Ar^+$ (Hattendorf and Günther, 2000). Suppression of $^{40}Ar^+$ allows the measurement of $^{40}Ca^+$ down to a detection limit of $\sim$10 μg/g in a 30-μm inclusion in quartz (Günther et al., 2001a).

dler et al., 2000; Kamenetsky et al., 2000, 2002; De Hoog et al., 2001). Uniquely, laser ablation can also sample whole melt inclusions inside a crystal. Their original composition can be re-integrated, even if they are devitrified and crystallized to a heterogeneous phase mixture. Quantitative LA-ICPMS analysis of enclosed glassy or crystallized melt inclusions below the sample surface follows the same principles as used for heterogeneous fluid inclusions (Fig. 11). The main difference is that melt inclusions not only form internal precipitates, but also may deposit a significant fraction of their initial mass as a (generally invisible) crystal layer onto the inside wall of the host crystal. Thermal re-homogenization of the inclusions is time-consuming and not always possible, and may require kinetic studies to achieve complete homogenization without excess host-mineral melting or volatile loss (Audétat et al., 2000b; Danyushevsky et al., 2002).

The mixed LA-ICPMS signal acquired from an initially unknown proportion of inclusion and host mineral can be numerically separated into contributions by the host and the original melt trapped at high temperature, without any physical treatment of the sample. The required equations and uncertainty calculations were derived by Halter et al. (2002a) for the general case of complex host minerals containing most or all of the elements in the inclusion, but in different concentrations. The quantification is applicable provided that (1) all major and minor elements are recorded in the same LA-ICPMS signal to allow normalization to a fixed oxide total, and (2) the concentration of one element in the original melt can be estimated independently and used as an internal standard. The ICPMS equipment therefore must be able to measure all light major elements including Na, Al and Ca. For small or relatively Ca-poor inclusions, dynamic reaction cell ICPMS can be useful, to suppress $^{40}Ar^+$ background on $^{40}Ca^+$ (Günther et al., 2001a; Fig. 15), but most melt inclusions of basic to intermediate composition are not limited in this regard (Halter et al., 2002a, 2003).

As a test of the quantification procedure for inclusions in host minerals containing several elements in comparable concentrations, we have studied glassy melt inclusions in plagioclase from a fresh basalt from the southern East Pacific Rise (sample ALV-3352-7, STOWA cruise 17°–19°S; Sinton, 1999). It contains minor olivine and $\sim$10 vol.% of small plagioclase phenocrysts with abundant melt-inclusions, in a completely fresh glassy matrix ($\sim$90 vol.%). This sample allows a comparison between matrix glass and melt inclusions, using both electron microprobe (EMP) and LA-ICPMS analyses, to illustrate the advantages as well as the limitations of both data sets.

For the matrix glass, major element analyses by EMP ($\sim$0.2–50 wt.%) and trace-element analyses by SIMS ($\sim$2–100 μg/g) are in excellent agreement ($\pm$3% RSD on average) with LA-ICPMS results obtained with a single 40-element menu (Fig. 7a). This shows that there is no systematic inconsistency in the calibrations for the three different analytical methods. Comparing the highly reproducible EMP data sets of matrix glass and melt inclusions (Fig. 16), however, a systematic difference is apparent. The inclusion glass is slightly but significantly enriched in Mg and Fe and depleted in Al, Ca and Na compared with the matrix glass. This could be explained by fractional crystallization of olivine and its separation from the plagioclase phenocrysts before extrusion of the basalt. Alternatively, it can be explained by in situ crystallization of $\sim$16% plagioclase from melt inclusions that initially had the same composition as the matrix glass. The latter seems more likely as

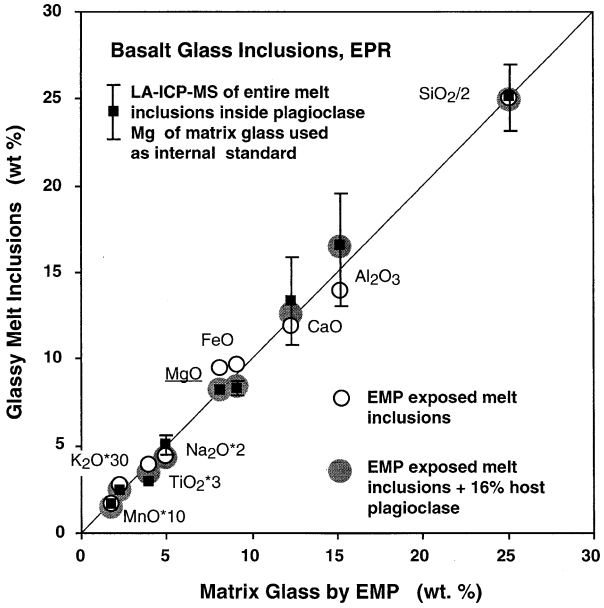

Fig. 16. Comparison of EMP and LA-ICPMS analyses of glassy melt inclusions in plagioclase (vertical axis) with the glassy groundmass (horizontal axis) of a fresh MOR basalt (Sample ALV-3352-7, EPR 17°–19°S, STOWA cruise, Sinton, 1999; see also Fig. 7a). All analyses agree within 10% relative deviation but in detail, EMP data for exposed melt inclusions (open circles) slightly deviate from the matrix glass with respect to elements that are compatible or incompatible in the host plagioclase. LA-ICPMS analysis of entire melt inclusions not exposed at the sample surface (filled squares with error bars denoting maximum uncertainties), calculated according to the procedure of Halter et al. (2002a) and using Mg of the matrix glass as internal standard, automatically accounts for ~16 wt.% sidewall growth of plagioclase from the melt inclusion after trapping. See text for discussion.

all melt inclusions have closely similar composition irrespective of their position in several plagioclase phenocrysts (variability is smaller than the size of the open circles in Fig. 16. The latter interpretation was used as the basis for the quantification of LA-ICPMS analyses of wholly enclosed melt inclusions in the same sample, by signal deconvolution and numerical reintegration of inclusion compositions (Halter et al., 2002a) and assuming the Mg concentration of the matrix glass as internal standard for the originally entrapped melt. The resulting melt concentrations (black squares in Fig. 16 agree, within their calculated uncertainties, with EMP analyses of exposed melt inclusions corrected by numerical addition of 16% plagioclase that may have crystallised onto the inclusion walls (grey circles in Fig. 16).

This agreement does not prove that the internal standardization of LA-ICPMS by normalization to Mg and the addition of plagioclase to the EMP analyses is the correct geochemical interpretation for the origin of this particular basalt. However, the example clearly shows that the ambiguity in interpretation applies equally to LA-ICPMS and EMP analyses and is, in fact, rather more relevant to EMP analyses because of their greater precision (Danyushevsky et al., 2002). The successful test for major elements in glassy inclusions, however, supports the credibility of LA-ICPMS analyses of crystallized inclusions. Careful heating/quenching experiments will remain an essential tool in many melt inclusion investigations, especially for the analysis of volatile components (H, C, F, S, Cl,. . .), but direct analysis of major to trace element concentrations of entire heterogeneous inclusions by LA-ICPMS offers to be a highly efficient complementary technique. It is particularly useful for geochemical studies of hydrous magmatic systems, where glassy melt inclusions are rare and not necessarily representative for the larger-scale magmatic process (Audétat and Pettke, 2003). The more hydrous melt inclusions commonly lose volatiles after entrapment and hence cannot be homogenised at the formation conditions, yet can still contain undisturbed major and trace element concentrations (Halter et al., in press).

4.6. Geochemical Applications

With its ability to quantitatively integrate complex transient signals and to record qualitative information about heterogeneous samples, LA-ICPMS has made a unique impact in studies of natural and synthetic fluid, melt and mineral inclusions in crystals. Since the early evaluation studies (e.g., Shepherd and Chenery, 1995), obtaining quantitative data on the metal concentrations of ore-forming hydrothermal fluids has been a particular challenge. Calibration of absolute concentrations by LA-ICPMS requires the right combination of laser and observation optical systems with an ICPMS with high sensitivity for trace-elements that is also capable of measuring Na over a large intensity range. With petrographic control on targeted ablation of individual inclusions, this technique has allowed the first quantitative reconstruction of evolving metal concentrations in successively trapped inclusion generations, before, during and after the precipitation of ore and gangue minerals in Sn-W-rich polymetallic vein deposits (Audétat et al., 1998, 2000a). Analyses of magmatic-hydrothermal brine and vapor inclusions demonstrated the extreme fractionation of certain elements between coexisting fluids of high and low salinity and density, indicating that high-temperature 'boiling' may be an active process of ore-metal separation (Heinrich et al., 1999). A previously unpublished dataset from a carbonatite-related hydrothermal REE deposit (Gakara, Burundi; Lehmann et al., 1994; Fig. 17) combines LA-ICPMS measurements of complete REE spectra of fluid inclusions in quartz and associated bastnaesite in veins. The high REE concentrations further illustrate the finding of Ulrich et al. (1999) and Audétat et al. (2000b) that relative ore-metal abundances in magmatic-hydrothermal ore deposits are primarily controlled by metal ratios in the ore-forming brines, but also by fractionation during mineral precipitation. LA-ICPMS was also used to analyse minor and trace element concentrations in dilute CO_2-rich late-metamorphic fluids in quartz (Griesser, 1999) and in diagenetic fluids in halite and carbonates (Shepherd et al., 1998, 2000; Ghazi and Shuttleworth, 1999). Quantitative analysis of fluid inclusions can be used to estimate thermodynamic data for mineral species from constraints imposed by element solubility in natural systems (Garofalo et al., 2000), and can provide critical input constraints for thermodynamic models of multicomponent fluid/rock reaction in ore-forming and other deeply exposed hydrothermal systems. Studies of silicate and sulfide melt inclusions are rapidly emerging, and the same quantification approach can also be applied to inclusions of one mineral in another. Thus, the ability of LA-ICPMS to obtain highly time-resolved phase-compositional information was a key to the

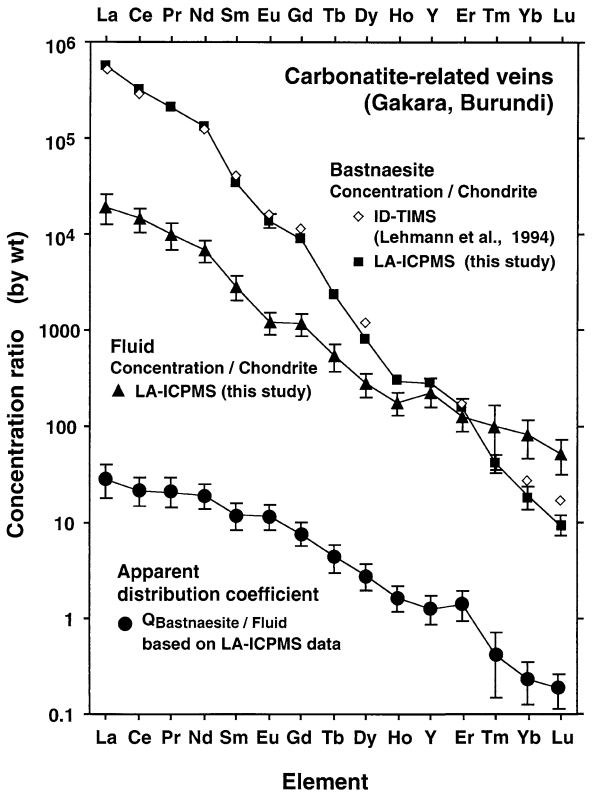

Fig. 17. Chondrite-normalized REE + Y concentrations of hypersaline fluid inclusions (~60 wt.% NaCl equivalent) and bastnaesite ([Ce, La,. . .]FCO_3) from carbonatite-related hydrothermal veins at Gakara (Burundi). The bastnaesite analysed by LA-ICPMS (black squares; reproducibility of 35 spot analyses within symbol size unless indicated by 1σ error bars) differs slightly from a sample analysed by ID-TIMS (open diamonds; Lehmann et al., 1994), possibly reflecting open-system REE fractionation during successive precipitation of bastnaesite from the fluid having a much flatter REE pattern. Bastnaesite and fluid inclusions were both analysed using SRM610 as external standard. Element concentrations in bastnaesite were calculated by molar normalization to an ideal stoichiometry of 100% $R(FCO_3)$, where R is the sum of all REE+Y. Absolute concentrations in fluid inclusions in associated quartz, obtained by using Na as internal standard with correction for K (Eqn. 5), range from 1.5 ± 0.3 wt.% Ce down to 4.1 ± 0.7 μg/g Tm. Besides very high and variable concentrations of REE, the fluid also contains ~2 wt.% Cu and Fe each, and minor U and Th. Error bars of fluid composition (triangles) denote 1σ variation among 13 pseudosecondary brine inclusions. Note that the fluid/mineral concentration ratio Q varies systematically over two orders of magnitude, indicating significant REE fractionation between fluids and hydrothermal minerals, similar to data obtained by Bühn et al. (1999) from the Kalkfeld carbonatite complex in Namibia.

discoveries by Ballhaus and Sylvester (2000) and Alard et al. (2000) that highly siderophile trace-metals in mantle peridotites and in the Merensky Reef PGE deposit of the Bushveld Igneous Complex are hosted by micro-inclusions of distinct PGE-rich sulfide and other accessory solid phases. A major area of future applications are experimental studies, using LA-ICPMS to analyse unquenchable fluid, melt and sulfide phases by trapping them in inert minerals at high temperatures and pressures, as shown for diverse conditions, chemical systems and experimental setups by Loucks and Mavrogenes (1999), Schäfer et al. (1999), and Stalder et al. (2001).

5. STRENGTHS, WEAKNESSES AND FUTURE DEVELOPMENTS

High-energy UV lasers with beam homogenization and aperture imaging optics have been a key to the latest microanalytical improvements in LA-ICPMS, because of the superior ablation performance of the short wavelength combined with a laterally even beam profile. Element fractionation has been reduced to the level of becoming negligible at the measurement precision (typically 2–5% RSD) inherent to sequential quadrupole detection obtained for transient signals from shallow ablation pits. The best laser ablation systems now allow matrix-insensitive cross-calibration between silicates, oxide minerals, silicate melts, hydrous fluids and probably even sulfides, as long as the particles of the aerosol are small enough to allow near-complete vaporization and ionization of the entire sample. LA-ICPMS permits depth profiling at ~0.1 μm vertical resolution, effectively destruction-free ablation of cut gemstones, rapid reconnaissance U-Pb geochronology of zircon, and quantitative ablation and reconstitution of the bulk composition of heterogeneous fluid, melt and mineral inclusions. Despite high ionization efficiency for most elements, the compositional complexity of many geological samples leads to significant ion cluster production in the ICP and in the mass-spectrometer interface. As a result, mass interferences restrict the limits of detection for certain elements such as Ca, S or Fe. Interferences caused by recombination of analyte ions with major plasma-gas ions (clusters with Ar, H, O, C,. . .) can be reduced or eliminated with the dynamic reaction cell (DRC) technology, which is likely to make a growing impact in future applications. Alternatively, interferences can be eliminated by high mass-resolution ICPMS. The resulting reduction in sensitivity is acceptable for some applications, and partly balanced by the high transmission efficiency and scanning speed of new magnetic-sector instruments. ICPMS has inherently poor sensitivity for some elements with high ionization potential, preventing analysis of F and limiting the detection of all other halogens. On the other hand, it is comparatively sensitive to light trace-elements such as Be, Li and B. LA-ICPMS challenges or exceeds the sensitivities of most other microprobe techniques for heavy elements. Routine detection limits are in the ng/g range for solids and μg/g range for typical fluid inclusions, and can be further improved with selective adjustment to longer acquisition times for masses with low abundance in a sample. Time-of-flight ICPMS combines multi-element capability across the entire mass range with slightly improved precision due to the effectively simultaneous data acquisition mode, but is unlikely to make a major impact until the sensitivity and dynamic range of the instruments can be drastically improved.

The most severe limitation of LA-ICPMS for certain applications is the need for an internal standard, which can lead to uncertainty in the calibration approach and prevent the calculation of absolute concentrations in some fluid inclusions. For Cl-rich aqueous inclusions, a rigorous description of the liquidus surfaces of ice, hydrohalite and halite in the respective multicomponent salt –water system may replace the simple approximation of NaCl equivalent wt.% (Eqn. 5) in the future. Thermodynamic models are already available for the H_2O-NaCl-$CaCl_2$-KCl subsystem (Spencer et al., 1990) which could be extended to include $FeCl_2$, higher temperatures and higher

salinities in excess of 30%, where systematic deviations from the simplified Eqn. 5 are probably greatest (Table 1).

Secondary ion mass spectrometry (SIMS) provides better signal stability compared with quadrupole LA-ICPMS (Shimizu and Hart, 1982). Therefore, SIMS is particularly suited for precise measurements of light stable isotopes (Eldridge et al., 1993; Chaussidon et al., 1997; Valley et al., 1998; McConville et al., 2000) and is routinely used for U/Pb geochronology (SHRIMP; Williams, 1998), although LA-ICPMS with matrix-matched standards is not much inferior for zircon geochronology any more (e.g., Belousova et al., 2001; Bruguier et al., 2001). The emergence of multiple-collector ICPMS in conjunction with laser ablation will offer unique advantages especially for in situ isotopic studies of elements with high ionization potential (e.g., Hirata and Yamaguchi, 1999). SIMS is well established and has unique advantages for some elements (notably H, C and other volatile elements), but accurate calibration depends on matrix-matched external standardization (i.e., standards and samples with closely similar major-element composition), because incomplete ionization by ion sputtering leads to strongly matrix-dependent backgrounds (Macrae, 1995). Also, SIMS is a comparatively slow and expensive technique, with a typical efficiency of ~10 point analyses per day depending on the number of elements to be analysed, compared with LA-ICPMS which permits up to ~100 point analyses per day. The slow sample removal rate and strong matrix dependence are the main reasons why SIMS analysis of fluid inclusions has not become practical (Diamond et al., 1990).

Proton-induced X-ray emission (Micro-PIXE) is the basis of a truly non-destructive trace-element microprobe with some unique advantages, but it does not achieve the sensitivity of LA-ICPMS for some light (Li, B, Na) and heavy (e.g., REE) elements (Ryan et al., 1995, 2001a; Bühn et al., 1999). High-energy protons have sufficient penetration depth to permit in situ analysis of fluid and melt inclusions beneath a sample surface, but detection of low-energy X-ray lines from light elements is limited by matrix absorbance. Recently, coupled micro-PIXE and PIGE (proton-induced γ-ray emission) have been explored to measure Na and especially F (Ryan et al., 2001a), an important element which is inaccessible to ICPMS except with a He source (Nam et al., 1996). Micro-PIXE has also been successfully used for exposed glassy melt inclusions (Dietrich et al., 2000), and is an ideal technique where high lateral resolution (~1 μm) is required. Scanning the proton beam across a subsurface fluid inclusion can map the trace-element distribution and permits standardless quantification of absolute element abundances in a given inclusion volume (Ryan et al., 1995, 2001b). Synchrotron-XRF offers similar possibilities (e.g., Vanko et al., 2001; Ménez et al., 2002; Mavrogenes et al., 2002), but application to solve geochemical problems seems to be constrained by sensitivity, and by cost and accessibility.

The combination of laser-ablation with optical emission spectrometry (LA-ICP-OES) remains potentially attractive as it offers a totally independent and simultaneous multi-element detection method (e.g., Moenke-Blankenburg et al., 1992; Kanicky and Mermet, 1996) that could be linked on-line with ICPMS. Attempts to analyse S and some major elements suffering from high backgrounds in ICPMS (notably Ca, Mg, Fe) in fluid inclusions have so far not been successful (Pettke et al., 2000), because the detectors in commercial ICP-OES instruments have insufficient sensitivity and dynamic range, and commercial instrument software does not permit satisfactory time-resolved acquisition for short transient signals. Laser-induced breakdown spectrometry (LIBS; Boiron et al., 1991) can be accurately calibrated for major cation ratios (e.g., Ca/K/Na; Dérome et al., in press) but may be difficult to extend to trace-element concentrations due to the expected strong matrix effects in the microplasma.

In summary, LA-ICPMS is a highly efficient technique for quantitative multi-element microanalysis across a large range of concentrations in very diverse sample types. It has unique advantages where high sensitivity for many elements needs to be combined with the possibility of integrating complex time-resolved signals, as in the analysis of polyphase inclusions in minerals. Thus, accurately re-constituted in situ analyses of homogeneous to highly heterogeneous materials with diverse matrices are obtained, provided that an internal standard or an element total can be defined. It must be noted, finally, that laser optical systems and commercial ICPMS instruments have significantly different specifications. The appropriate combination of instrumentation will remain the key to successfully applying the technique to a particular geochemical question.

Acknowledgments—We would like to thank Simon Jackson and Uwe Wiechert for discussion and helpful comments about earlier versions of this manuscript. Rolf Frischknecht and Thomas Ulrich have contributed to earlier projects on which the experience summarized in this paper builds. Our biggest 'thank-you' goes to Urs Menet who has been an essential helper throughout the technical development and continuing upgrade of our LA-ICPMS facility. We are grateful to Eric Reusser for the continued maintenance of and support at ETH Zürich's electron microprobe lab, to Graham Layne at WHOI for his assistance during ion probe analysis, and to Ulrich Hein, Bernd Lehmann and David Banks for contributing test samples. Very constructive and careful reviews by Robert Burruss, Larryn Diamond, Stephen Eggins and Paul Sylvester have helped to improve the scientific balance and presentation of this paper. This research was funded by ETH Zürich and the Swiss National Science Foundation through several grants since 1996, which are gratefully acknowledged.

Associate editor: R. C. Burruss

REFERENCES

Alard O., Griffin W. L., Lorand J. P., Jackson S. E., and O'Reilly S. Y. (2000) Non-chondritic distribution of the highly siderophile elements in mantle sulphides. *Nature* **407**(6806), 891–894.

Audétat A. and Pettke T. (2003) The magmatic-hydrothermal evolution of two barren granites: A melt and fluid inclusion study of the Rito del Medio and Cañada Pinabete plutons in northern New Mexico (USA). *Geochim. Cosmochim. Acta* **67,** 97–121.

Audétat A., Günther D., and Heinrich C. A. (1998) Formation of a magmatic-hydrothermal ore deposit: Insights with LA-ICP-MS analysis of fluid inclusions. *Science* **279**(5359), 2091–2094.

Audétat A., Günther D., and Heinrich C. A. (2000a) Causes for large-scale metal zonation around mineralized plutons: Fluid inclusion LA-ICP-MS evidence from the Mole Granite, Australia. *Econ. Geol.* **95**(8), 1563–1581.

Audétat A., Günther D., and Heinrich C. A. (2000b) Magmatic-hydrothermal evolution in a fractionating granite: A microchemical study of the Sn-W-F-mineralized Mole Granite (Australia). *Geochim. Cosmochim. Acta* **64,** 3373–3393.

Axelsson M. D. and Rodushkin I. (2001) Determination of major and trace elements in sphalerite using laser ablation double focusing sector field ICP-MS. *J. Geochem. Explor.* **72**(2), 81–89.

Ballhaus C. and Sylvester P. (2000) Noble metal enrichment processes in the Merensky Reef, Bushveld Complex. *J. Petrol.* **41**(4), 545–561.

Bandura D. R., Baranov V. I., and Tanner S. D. (2001) Reaction chemistry and collisional processes in multipole devices for resolving isobaric interferences in ICP-MS. *Fresenius' J. Anal. Chem.* **370**(5), 454–470.

Becker J. S. and Dietze H. J. (2000) Precise and accurate isotope ratio measurements by ICP-MS. *Fresenius' J. Anal. Chem.* **368**(1), 23–30.

Belousova E. A., Griffin W. L., Shee S. R., Jackson S. E., and O'Reilly S. Y. (2001) Two age populations of zircons from the Timber Creek kimberlites, Northern Territory, as determined by laser-ablation ICP-MS analysis. *Aust. J. Earth Sci.* **48**(5), 757–765.

Bleiner D. and Günther D. (2001) Theoretical description and experimental observation of aerosol transport processes in laser ablation inductively coupled plasma mass spectrometry. *J. Anal. At. Spectrom.* **16**(5), 449–456.

Bleiner D., Hametner K., and Günther D. (2000a) Optimization of a laser ablation-inductively coupled plasma "time of flight" mass spectrometry system for short transient signal acquisition. *Fresenius' J. Anal. Chem.* **368**(1), 37–44.

Bleiner D., Plotnikov A., Vogt C., Wetzig K., and Günther D. (2000b) Depth profile analysis of various titanium based coatings on steel and tungsten carbide using laser ablation inductively coupled plasma–"time of flight" mass spectrometry. *Fresenius' J. Anal. Chem.* **368**(2–3), 221–226.

Bodnar R. J. and Vityk M. O. (1994) Interpretation of microthermometric data for H_2O-NaCl fluid inclusions. In *Fluid Inclusions in Minerals* (eds. B. DeVivo and M. L. Frezzotti), pp. 117–130. Virginia Tech, Blacksburg.

Boiron M. C., Dubessy J., Andre N., Briand A., Lacour J. L., Mauchien P., and Mermet J. M. (1991) Analysis of mono-atomic ions in individual fluid inclusions by laser-produced plasma emission-spectroscopy. *Geochim. Cosmochim. Acta* **55,** 917–923.

Boulyga S. F. and Becker J. S. (2001) ICP-MS with hexapole collision cell for isotope ratio measurements of Ca, Fe, and Se. *Fresenius' J. Anal. Chem.* **370**(5), 618–623.

Bruguier O., Telouk P., Cocherie A., Fouillac A. M., and Albarede F. (2001) Evaluation of Pb-Pb and U-Pb laser ablation ICP-MS zircon dating using matrix-matched calibration samples with a frequency quadrupled (266 nm) Nd-YAG laser. *Geostand. Newsl.—J. Geostand. Geoanal.* **25**(2–3), 361–373.

Bryant C. J., Arculus R. J., and Eggins S. M. (1999) Laser ablation-inductively coupled plasma-mass spectrometry and tephras: A new approach to understanding arc-mama genesis. *Geology* **27**(12), 1119–1122.

Bühn B., Rankin A. H., Radtke M., Haller M., and Knochel A. (1999) Burbankite, a (Sr,REE,Na,Ca)-carbonate in fluid inclusions from carbonatite-derived fluids: Identification and characterization using laser Raman spectroscopy, SEM-EDX, and synchrotron micro-XRF analysis. *Am. Mineral.* **84**(7–8), 1117–1125.

Callies G., Schittenhelm H., Berger P., and Hugel H. (1998) Modeling of the expansion of laser-evaporated matter in argon, helium and nitrogen and the condensation of clusters. *Appl. Surf. Sci.* **129,** 134–141.

Campana S. E., Thorrold S. R., Jones C. M., Günther D., Tubrett M., Longerich H., Jackson S., Halden N. M., Kalish J. M., Piccoli P., dePontual H., Troadec H., Panfili J., Secor D. H., Severin K. P., Sie S. H., Thresher R., Teesdale W. J., and Campbell J. L. (1997) Comparison of accuracy, precision, and sensitivity in elemental assays of fish otoliths using the electron microprobe, proton-induced X-ray emission, and laser ablation inductively coupled plasma mass spectrometry. *Can. J. Fisheries Aquat. Sci.* **54**(9), 2068–2079.

Chaussidon M., Robert F., Mangin D., Hanon P., and Rose E. F. (1997) Analytical procedures for the measurement of boron isotope compositions by ion microprobe in meteorites and mantle rocks. *Geostand. Newsl.—J. Geostand. Geoanal.* **21**(1), 7–17.

Christensen J. N., Halliday A. N., Lee D. C., and Hall C. M. (1995) In-situ Sr isotopic analysis by laser-ablation. *Earth Planet. Sci. Lett.* **136**(1–2), 79–85.

Cullen J. T., Field M. P., and Sherrell R. M. (2001) Determination of trace elements in filtered suspended marine particulate material by sector field HR-ICP-MS. *J. Anal. At. Spectrom.* **16**(11), 1307–1312.

Danyushevsky L. V., McNeill A. W., and Sobolev A. V. (2002) Experimental and petrological studies of melt inclusions in phenocrysts from mantle-derived magmas: An overview of techniques, advantages and complications. *Chem. Geol.* **183**(1–4), 5–24.

Darke S. A. and Tyson J. F. (1993) Interaction of laser-radiation with solid materials and its significance to analytical spectrometry—A review. *J. Anal. At. Spectrom.* **8**(2), 145–209.

Davidson J., Tepley F., Palacz Z., and Meffan-Main S. (2001) Magma recharge, contamination and residence times revealed by in situ laser ablation isotopic analysis of feldspar in volcanic rocks. *Earth Planet. Sci. Lett.* **184**(2), 427–442.

De Hoog J. C. M., Mason P. R. D., and van Bergen M. J. (2001) Sulfur and chalcophile elements in subduction zones: Constraints from a laser ablation ICP-MS study of melt inclusions from Galunggung Volcano, Indonesia. *Geochim. Cosmochim. Acta* **65,** 3147–3164.

Dérome D., Cathelineau M., Cuney M., Fabre C., and Lhomme T. (in press) Evidence of brine mixing in the McArthur River unconformity-type uranium deposit (Saskatchewan, Canada). *Econ. Geol.*

Diamond L. W. (1994) Salinity of multivolatile fluid inclusions determined from clathrate hydrate stability. *Geochim. Cosmochim. Acta* **58,** 19–41.

Diamond L. W., Marshall D. D., Jackman J. A., and Skippen G. B. (1990) Elemental analysis of individual fluid inclusions in minerals by secondary ion mass-spectrometry (SIMS)—Application to cation ratios of fluid inclusions in an Archean Mesothermal gold-quartz vein. *Geochim. Cosmochim. Acta* **54,** 545–552.

Dietrich A., Lehmann B., and Wallianos A. (2000) Bulk rock and melt inclusion geochemistry of Bolivian tin porphyry systems. *Econ. Geol.* **95**(2), 313–326.

Durrant S. F. (1999) Laser ablation inductively coupled plasma mass spectrometry: Achievements, problems, prospects. *J. Anal. At. Spectrom.* **14**(9), 1385–1403.

Eggins S. M., Kinsley L. P. J., and Shelley J. M. G. (1998a) Deposition and element fractionation processes during atmospheric pressure laser sampling for analysis by ICP-MS. *Appl. Surf. Sci.* **129,** 278–286.

Eggins S. M., Rudnick R. L., and McDonough W. F. (1998b) The composition of peridotites and their minerals: A laser-ablation ICP-MS study. *Earth Planet. Sci. Lett.* **154**(1–4), 53–71.

Eldridge C. S., Williams N., and Walshe J. L. (1993) Sulfur isotope variability in sediment-hosted massive sulfide deposits as determined using the ion microprobe SHRIMP. 2. A study of the HYC deposit at McArthur River, Northern-Territory, Australia. *Econ. Geol.* **88**(1), 1–26.

Fiebig J., Wiechert U., Ruble D., and Hoefs J. (1999) High-precision in situ oxygen isotope analysis of quartz using an ArF laser. *Geochim. Cosmochim. Acta* **63,** 687–702.

Figg D. J., Cross J. B., and Brink C. (1998) More investigations into elemental fractionation resulting from laser ablation inductively coupled plasma mass spectrometry on glass samples. *Appl. Surf. Sci.* **129,** 287–291.

Fryer B. J., Jackson S. E., and Longerich H. P. (1995) Design, operation and role of the laser-ablation microprobe coupled with an inductively-coupled plasma-mass-spectrometer (LAM-ICP-MS) in the earth-sciences. *Can. Mineral.* **33,** 303–312.

Garofalo P., Audétat A., Günther D., Heinrich C. A., and Ridley J. (2000) Estimation and testing of standard molar thermodynamic properties of tourmaline end-members using data of natural samples. *Am. Mineral.* **85**(1), 78–88.

Gerson A. R., Lange A. G., Prince K. E., and Smart R. S. (1999) The mechanism of copper activation of sphalerite. *Appl. Surf. Sci.* **137**(1–4), 207–223.

Ghazi A. M. and Shuttleworth S. (1999) Trace element determination of single fluid inclusions by laser ablation ICP-MS: Applications for halites from sedimentary basins. *Analyst* **125**(1), 205–210.

Ghazi A. M., Shuttleworth S., Angulo S. J., and Pashley D. H. (2000) New applications for laser ablation high resolution ICPMS (LA-HR-ICP-MS): Quantitative measurements of gallium diffusion across human root dentin. *J. Anal. At. Spectrom.* **15**(10), 1335–1341.

Ghazi A. M., Wataha J. C., O'Dell N. L., Singh B. B., Simmons R., and Shuttleworth S. (2002) Quantitative concentration profiling of nickel in tissues around metal implants: a new biomedical application of

laser ablation sector field ICP-MS. *J. Anal. At. Spectrom.* **17**(10), 1295–1299.

Goldstein R. H. and Reynolds T. J. (1994) Systematics of fluid inclusions in diagenetic minerals. *Soc. Sediment. Geol. Short Course Series* **31,** 199.

Gray A. L. (1985) Solid sample introduction by laser ablation for inductively coupled plasma source-mass spectrometry. *Analyst* **110**(5), 551–556.

Griesser A (1999) *Fluidchemie und hydrothermale Nebengesteinsveränderungen von Klüften im östlichen Val Piora (TI, Schweiz).* M.Sc. thesis, ETH.

Griffin W. L., Pearson N. J., Belousova E., Jackson S. E., van Achterbergh E., O'Reilly S. Y., and Shee S. R. (2000) The Hf isotope composition of cratonic mantle: LAM-MC-ICPMS analysis of zircon megacrysts in kimberlites. *Geochim. Cosmochim. Acta* **64,** 133–147.

Guillong M. and Günther D. (2001) Quasi "non-destructive" laser ablation-inductively coupled plasma-mass spectrometry fingerprinting of sapphires. *Spectrochim. Acta B—At. Spectrosc.* **56**(7), 1219–1231.

Guillong M. and Günther D. (2002) Effect of particle size distribution on ICP-induced elemental fractionation in laser ablation-inductively coupled plasma-mass spectrometry. *J. Anal. At. Spectrom.* **17**(8), 831–837.

Guillong M., Horn I., and Günther D. (2002) Capabilities of a homogenized 266 nm Nd: YAG laser ablation systems for LA-ICP-MS. *J. Anal. At. Spectrom.* **17,** 8–14.

Günther D. (2002) Laser ablation-inductively coupled plasma mass spectrometry, trends. *J. Anal. Bioanal. Chem.* **372**(1), 31–32.

Günther D. and Heinrich C. A. (1999a) Enhanced sensitivity in laser ablation-ICP mass spectrometry using helium-argon mixtures as aerosol carrier—Plenary lecture. *J. Anal. At. Spectrom.* **14**(9), 1363–1368.

Günther D. and Heinrich C. A. (1999b) Comparison of the ablation behaviour of 266 nm Nd: YAG and 193 nm ArF excimer lasers for LA-ICP-MS analysis. *J. Anal. At. Spectrom.* **14**(9), 1369–1374.

Günther D., Frischknecht R., Heinrich C. A., and Kahlert H. J. (1997a) Capabilities of an argon fluoride 193 nm excimer laser for laser ablation inductively coupled plasma mass spectrometry microanalysis of geological materials. *J. Anal. At. Spectrom.* **12**(9), 939–944.

Günther D., Frischknecht R., Muschenborn H. J., and Heinrich C. A. (1997b) Direct liquid ablation: A new calibration strategy for laser ablation ICP-MS microanalysis of solids and liquids. *Fresenius' J. Anal. Chem.* **359**(4–5), 390–393.

Günther D., Audétat A., Frischknecht R., and Heinrich C. A. (1998) Quantitative analysis of major, minor and trace elements in fluid inclusions using laser ablation inductively coupled plasma mass spectrometry. *J. Anal. At. Spectrom.* **13**(4), 263–270.

Günther D., Jackson S. E., and Longerich H. P. (1999) Laser ablation and arc/spark solid sample introduction into inductively coupled plasma mass spectrometers. *Spectrochim. Acta B—At. Spectrosc.* **54**(3–4), 381–409.

Günther D., Horn I., and Hattendorf B. (2000) Recent trends and developments in laser ablation-ICP-mass spectrometry. *Fresenius' J. Anal. Chem.* **368**(1), 4–14.

Günther D., Hattendorf B., and Audétat A. (2001a) Multi-element analysis of melt and fluid inclusions with improved detection capabilities for Ca and Fe using laser ablation with a dynamic reaction cell ICP-MS. *J. Anal. At. Spectrom.* **16,** 1085–1090.

Günther D., von Quadt A., Wirz R., Cousin H., and Dietrich V. J. (2001b) Elemental analyses using laser ablation-inductively coupled plasma-mass spectrometry (LA-ICP-MS) of geological samples fused with $Li_2B_4O_7$ and calibrated without matrix-matched standards. *Mikrochim. Acta* **136**(3–4), 101–107.

Halliday A. N., Lee D. C., Christensen J. N., Rehkamper M., Yi W., Luo X. Z., Hall C. M., Ballentine C. J., Pettke T., and Stirling C. (1998) Applications of multiple collector-ICPMS to cosmochemistry, geochemistry, and paleoceanography. *Geochim. Cosmochim. Acta* **62,** 919–940.

Halter W. E., Pettke T., Heinrich C. A., and Rothen-Rutishauser B. (2002a) Major to trace element analysis of melt inclusions by laser-ablation ICP-MS: Methods of quantification. *Chem. Geol.* **183**(1–4), 63–86.

Halter W. E., Pettke T., and Heinrich C. A. (2002b) The origin of Cu/Au ratios in porphyry-type ore deposits. *Science* **296**(5574), 1844–1846.

Halter W., Pettke T., and Heinrich C. A. (in press) Structure and evolution of an andesitic magma chamber: Insight form laser-ablation ICP-MS of melt inclusions in an andesitic complex I: Analytical approach and data evaluation. *Contrib. Mineral. Petrol*.

Hattendorf B. and Günther D. (2000) Characteristics and capabilities of an ICP-MS with a dynamic reaction cell for dry aerosols and laser ablation. *J. Anal. At. Spectrom.* **15**(9), 1125–1131.

Hattendorf B. and Günther D. (2001) Experimental evidence for the formation of doubly charged oxide and hydroxide ions in inductively coupled plasma mass spectrometry. *Fresenius' J. Anal. Chem.* **370**(5), 483–487.

Hattendorf B., Günther D., Schönbachler M., and Halliday A. N. (2001) Simultaneous ultra trace determination of Zr and Nb in chromium matrices with ICP-DRCMS. *Anal. Chem.* **73,** 5494–5498.

Heinrich C. A., Ryan C. G., Mernagh T. P., and Eadington P. J. (1992) Segregation of ore metals between magmatic brine and vapor—A fluid inclusion study using pixe microanalysis. *Econ. Geol.* **87**(6), 1566–1583.

Heinrich C. A., Günther D., Audétat A., Ulrich T., and Frischknecht R. (1999) Metal fractionation between magmatic brine and vapor, determined by microanalysis of fluid inclusions. *Geology* **27**(8), 755–758.

Hermann J., Müntener O., and Günther D. (2001) Differentiation of mafic magma in a continental crust-to-mantle transition zone. *J. Petrol.* **42**(1), 189–206.

Hieftje G. M., Myers D. P., Li G. Q., Mahoney P. P., Burgoyne T. W., Ray S. J., and Guzowski J. P. (1997) Toward the next generation of atomic mass spectrometers—Plenary lecture. *J. Anal. At. Spectrom.* **12**(3), 287–292.

Hirata T. (2001) Determinations of Zr isotopic composition and U-Pb ages for terrestrial and extraterrestrial Zr-bearing minerals using laser ablation-inductively coupled plasma mass spectrometry: Implications for Nb-Zr isotopic systematics. *Chem. Geol.* **176**(1–4), 323–342.

Hirata T. and Nesbitt R. W. (1995) U-Pb isotope geochronology of zircon—Evaluation of the laser probe-inductively coupled plasma-mass spectrometry technique. *Geochim. Cosmochim. Acta* **59,** 2491–2500.

Hirata T. and Nesbitt R. W. (1997) Distribution of platinum group elements and rhenium between metallic phases of iron meteorites. *Earth Planet. Sci. Lett.* **147**(1–4), 11–24.

Hirata T. and Yamaguchi T. (1999) Isotopic analysis of zirconium using enhanced sensitivity-laser ablation-multiple collector-inductively coupled plasma mass spectrometry. *J. Anal. At. Spectrom.* **14**(9), 1455–1459.

Hirata T. and Ohno T. (2001) In-situ isotopic ratio analysis of iron using laser ablation-multiple collector-inductively coupled plasma mass spectrometry (LA-MC-ICP-MS). *J. Anal. At. Spectrom.* **16**(5), 487–491.

Horn E. E. and Tye C. T. (1989) Analysis of fluid inclusions in minerals by VG laser ablation ICP-MS. Second Biennial Pan-American Conference on Research on Fluid Inclusions, PACROFI II Abstracts, 32.

Horn I., Hinton R. W., Jackson S. E., and Longerich H. P. (1997) Ultra-trace element analysis of NIST SRM 616 and 614 using laser ablation microprobe inductively coupled plasma mass spectrometry (LAM-ICP-MS): A comparison with secondary ion mass spectrometry (SIMS). *Geostand. Newsl.—J. Geostand. Geoanal.* **21**(2), 191–203.

Horn I., Rudnick R. L., and McDonough W. F. (2000) Precise elemental and isotope ratio determination by simultaneous solution nebulization and laser ablation-ICP-MS: Application to U-Pb geochronology. *Chem. Geol.* **167**(3–4), 403–419.

Horn I., Guillong M., and Günther D. (2001) Wavelength dependant ablation rates for metals and silicate glasses using homogenized laser beam profiles—Implications for LA-ICP-MS. *Appl. Surf. Sci.* **182,** 91–102.

Jackson S., Pearson N. J., and Griffin W. L. (2001) In situ isotope ratio determination using laser-ablation (LA)-magnetic sector ICP-MS. In

Short Course Series, Vol. 29 (ed. P. Sylvester), pp. 105–119. Mineralogical Association of Canada.

Jackson S. E., Longerich H. P., Dunning G. R., and Fryer B. J. (1992) The application of laser-ablation microprobe-inductively coupled plasma-mass-spectrometry (LAM-ICP-MS) to in situ trace-element determinations in minerals. *Can. Mineral.* **30,** 1049–1064.

Jeffries T. E., Pearce N. J. G., Perkins W. T., and Raith A. (1996) Chemical fractionation during infrared and ultraviolet laser ablation inductively coupled plasma mass spectrometry—Implications for mineral microanalysis. *Anal. Commun.* **33**(1), 35–39.

Jeffries T. E., Jackson S. E., and Longerich H. P. (1998) Application of a frequency quintupled Nd:YAG source (lambda = 213 nm) for laser ablation inductively coupled plasma mass spectrometric analysis of minerals. *J. Anal. At. Spectrom.* **13**(9), 935–940.

Jenner G. A., Foley S. F., Jackson S. E., Green T. H., Fryer B. J., and Longerich H. P. (1993) Determination of partition-coefficients for trace-elements in high-pressure temperature experimental run products by laser-ablation microprobe inductively-coupled plasma-mass spectrometry (LAM-ICP-MS). *Geochim. Cosmochim. Acta* **57,** 5099–5103.

Kamenetsky V. S., Everard J. L., Crawford A. J., Varne R., Eggins S. M., and Lanyon R. (2000) Enriched end-member of primitive MORB melts: Petrology and geochemistry of glasses from Macquarie Island (SW Pacific). *J. Petrol.* **41**(3), 411–430.

Kamenetsky V. S., Sobolev A. V., Eggins S. M., Crawford A. J., and Arculus R. J. (2002) Olivine-enriched melt inclusions in chromites from low-Ca boninites, Cape Vogel, Papua New Guinea: Evidence for ultramafic primary magma, refractory mantle source and enriched components. *Chem. Geol.* **183**(1–4), 287–303.

Kanicky V. and Mermet J. M. (1996) Selection of internal standards for analysis of silicate rocks and limestones by laser ablation inductively coupled plasma atomic emission spectrometry (LA-ICP-AES). *Fresenius' J. Anal. Chem.* **355**(7–8), 887–888.

Kanicky V., Novotny I., Musil J., and Mermet J. M. (1997) Depth profiling of thick layers of graded metal zirconia ceramic coatings using laser ablation inductively coupled plasma atomic emission spectrometry. *Appl. Spectrosc.* **51**(7), 1042–1046.

Knudsen T. L., Griffin W. L., Hartz E. H., Andresen A., and Jackson S. E. (2001) In-situ hafnium and lead isotope analyses of detrital zircons from the Devonian sedimentary basin of NE Greenland: A record of repeated crustal reworking. *Contrib. Mineral. Petrol.* **141**(1), 83–94.

Latkoczy C. and Günther D. (2002) Enhanced sensitivity in inductively coupled plasma sector field mass spectrometry for direct solid analysis using laser ablation (LA-ICP-SFMS). *J. Anal. At. Spectrom.* **17**(10), 1264–1270.

Lehmann B., Nakai S., Hohndorf A., Brinckmann J., Dulski P., Hein U. F., and Masuda A. (1994) REE mineralization at Gakara, Burundi—Evidence for anomalous upper-mantle in the Western Rift-Valley. *Geochim. Cosmochim. Acta* **58,** 985–992.

Liu H. C., Borisov O. V., Mao X. L., Shuttleworth S., and Russo R. E. (2000) Pb/U fractionation during Nd:YAG 213 nm and 266 nm laser ablation sampling with inductively coupled plasma mass spectrometry. *Appl. Spectrosc.* **54**(10), 1435–1442.

Longerich H. P., Günther D., and Jackson S. E. (1996a) Elemental fractionation in laser ablation inductively coupled plasma mass spectrometry. *Fresenius' J. Anal. Chem.* **355**(5–6), 538–542.

Longerich H. P., Jackson S. E., and Günther D. (1996b) Laser ablation inductively coupled plasma mass spectrometric transient signal data acquisition and analyte concentration calculation. *J. Anal. At. Spectrom.* **11**(9), 899–904.

Longerich H. P., Jackson S. E., and Günther D. (1997) Laser ablation inductively coupled plasma mass spectrometric transient signal data acquisition and analyte concentration calculation (Vol 11, pg 899, 1996). *J. Anal. At. Spectrom.* **12**(3), 391–391.

Loucks R. R. and Mavrogenes J. A. (1999) Gold solubility in supercritical hydrothermal brines measured in synthetic fluid inclusions. *Science* **284**(5423), 2159–2163.

Machado N. and Simonetti A. (2001) U-Pb dating and Hf isotopic composition of zircon by laser-ablation-MC-ICP-MS. In *Short Course Series, Vol. 29* (ed. P. Sylvester), pp. 121–146. Mineralogical Association of Canada.

Macrae N. D. (1995) Secondary-ion mass-spectrometry and geology. *Can. Mineral.* **33,** 219–236.

Mahoney P. P., Li G. Q., and Hieftje G. M. (1996) Laser ablation-inductively coupled plasma mass spectrometry with a time-of-flight mass analyser. *J. Anal. At. Spectrom.* **11**(6), 401–405.

Mank A. J. G. and Mason P. R. D. (1999) A critical assessment of laser ablation ICP-MS as an analytical tool for depth analysis in silica-based glass samples. *J. Anal. At. Spectrom.* **14**(8), 1143–1153.

Mason P. (2001) Expanding the capabilities of laser-ablation ICP-MS with collision and reaction cells. In *Short Course Series, Vol. 29* (ed. P. Sylvester), pp. 63–81. Mineralogical Association of Canada.

Mason P. and Mank A. J. G. (2001) Depth analysis by laser-ablation ICP-MS. In *Short Course Series, Vol. 29* (ed. P. Sylvester), pp. 93–103. Mineralogical Association of Canada.

Mavrogenes J. A., Berry A. J., Newville M., and Sutton S. R. (2002) Copper speciation in vapor-phase fluid inclusions from the Mole Granite, Australia. *Am. Mineral.* **87**(10), 1360–1364.

McConville P., Boyce A. J., Fallick A. E., Harte B., and Scott E. M. (2000) Sulphur isotope variations in diagenetic pyrite from core plug to sub-millimetre scales. *Clay Mineral.* **35**(1), 303–311.

Ménez B., Philippot P., Bonnin-Mosbah M., Simionovici A., and Gibert F. (2002) Analysis of individual fluid inclusions using synchrotron X-ray fluorescence microprobe: Progress toward calibration for trace elements. *Geochim. Cosmochim. Acta* **66,** 561–576.

Moenke-Blankenburg L. and Günther D. (1992) Laser microanalysis of geological samples by atomic emission spectrometry (LM-AES) and inductively coupled plasma atomic emission-spectrometry (LM-ICP-AES). *Chem. Geol.* **95**(1–2), 85–92.

Moenke-Blankenburg L., Schumann T., Günther D., Kuss H. M., and Paul M. (1992) Quantitative-analysis of glass using inductively coupled plasma atomic emission and mass-spectrometry, laser microanalysis inductively coupled plasma atomic emission-spectrometry and laser ablation inductively coupled plasma mass-spectrometry. *J. Anal. At. Spectrom.* **7**(2), 251–254.

Moenke-Blankenburg L., Schumann T., and Nolte J. (1994) Direct solid soil analysis by laser-ablation inductively-coupled plasma-atomic emission-spectrometry. *J. Anal. At. Spectrom.* **9**(9), 1059–1062.

Moissette A., Shepherd T. J., and Chenery S. R. (1996) Calibration strategies for the elemental analysis of individual aqueous fluid inclusions by laser ablation inductively coupled plasma mass spectrometry. *J. Anal. At. Spectrom.* **11**(3), 177–185.

Nam S. H., Zhang H., Cai M. X., Lim J. S., and Montaser A. (1996) Status report on helium inductively coupled plasma mass spectrometry. *Fresenius' J. Anal. Chem.* **355**(5–6), 510–520.

Nesbitt R. W., Hirata T., Butler I. B., and Milton J. A. (1997) UV laser ablation ICP-MS: Some applications in the earth sciences. *Geostand. Newsl.—J. Geostand. Geoanal.* **21**(2), 231–243.

Noronha F., Lourenço A., and Banks D. A. (2001) The tungsten-tin ore deposit of Panasqueira, Portugal. In *Mineral Deposits: Processes to Processing, Vol. 1* (ed. S. C.), pp. 75–78. Balkema.

Odegard M. and Hamester M. (1997) Preliminary investigation into the use of a high resolution inductively coupled plasma-mass spectrometer with laser ablation for bulk analysis of geological materials fused with $Li_2B_4O_7$. *Geostand. Newsl.—J. Geostand. Geoanal.* **21**(2), 245–252.

Pearce N. J. G., Perkins W. T., Abell I., Duller G. A. T., and Fuge R. (1992) Mineral microanalysis by laser ablation inductively coupled plasma mass-spectrometry. *J. Anal. At. Spectrom.* **7**(1), 53–57.

Perkins W. T., Fuge R., and Pearce N. J. G. (1991) Quantitative-analysis of trace-elements in carbonates using laser ablation inductively coupled plasma mass-spectrometry. *J. Anal. At. Spectrom.* **6**(6), 445–449.

Perkins W. T., Pearce N. J. G., and Jeffries T. E. (1993) Laser ablation inductively coupled plasma mass-spectrometry—A new technique for the determination of trace and ultra-trace elements in silicates. *Geochim. Cosmochim. Acta* **57,** 475–482.

Perkins W. T., Pearce N. J. G., and Westgate J. A. (1997) The development of laser ablation ICP-MS and calibration strategies: Examples from the analysis of trace elements in volcanic glass shards and sulfide minerals. *Geostand. Newsl.—J. Geostand. Geoanal.* **21**(2), 175–190.

Pettke T., Heinrich C. A., Ciocan A. C., and Günther D. (2000) Quadrupole mass spectrometry and optical emission spectroscopy: Detection capabilities and representative sampling of short transient signals from laser-ablation. *J. Anal. At. Spectrom.* **15**(9), 1149–1155.

Plotnikov A., Vogt C., Hoffmann V., Taschner C., and Wetzig K. (2001) Application of laser ablation inductively coupled plasma quadrupole mass spectrometry (LA-ICP-QMS) for depth profile analysis. *J. Anal. At. Spectrom.* **16**(11), 1290–1295.

Poitrasson F., Chenery S., and Shepherd T. J. (2000) Electron microprobe and LA-ICP-MS study of monazite hydrothermal alteration: Implications for U-Th-Pb geochronology and nuclear ceramics. *Geochim. Cosmochim. Acta* **64,** 3283–3297.

Ramsey M. H., Coles B. J., Wilkinson J. J., and Rankin A. H. (1992) Single fluid inclusion analysis by laser ablation inductively coupled plasma atomic emission-spectrometry—Quantification and validation. *J. Anal. At. Spectrom.* **7**(4), 587–593.

Rankin A. H., Ramsey M. H., Coles B., Vanlangevelde F., and Thomas C. R. (1992) The composition of hypersaline, iron-rich granitic fluids based on laser-ICP and synchrotron-XRF microprobe analysis of individual fluid inclusions in topaz, Mole Granite, Eastern Australia. *Geochim. Cosmochim. Acta* **56,** 67–79.

Russo R. E., Mao X. L., Borisov O. V., and Liu H. C. (2000) Influence of wavelength on fractionation in laser ablation ICP-MS. *J. Anal. At. Spectrom.* **15**(9), 1115–1120.

Ryan C. G., Heinrich C. A., Vanachterbergh E., Ballhaus C., and Mernagh T. P. (1995) Microanalysis of ore-forming fluids using the scanning proton microprobe. *Nucl. Instrum. Meth. Phys. Res. B—Beam Interac. Mat. Atoms* **104**(1–4), 182–190.

Ryan C. G., Jamieson D. N., Griffin W. L., Cripps G., and Szymanski R. (2001a) The new CSIRO-GEMOC nuclear microprobe. First results, performance and recent applications. *Nucl. Instrum. Meth. Phys. Res. B—Beam Interac. Mat. Atoms* **181,** 12–19.

Ryan C. G., van Achterbergh E., Griffin W. L., Pearson N. J., O'Reilly S. Y., and Kivi K. (2001b) Nuclear microprobe analysis of melt inclusions in minerals: Windows on metasomatic processes in the earth's mantle. *Nucl. Instrum. Meth. Phys. Res. B—Beam Interac. Mat. Atoms* **181,** 578–585.

Schäfer B., Frischknecht R., Günther D., and Dingwell D. B. (1999) Determination of trace-element partitioning between fluid and melt using LA-ICP-MS analysis of synthetic fluid inclusions in glass. *Eur. J. Mineral.* **11**(3), 415–426.

Sha L. K. and Chappell B. W. (1999) Apatite chemical composition, determined by electron microprobe and laser-ablation inductively coupled plasma mass spectrometry, as a probe into granite petrogenesis. *Geochim. Cosmochim. Acta* **63,** 3861–3881.

Shepherd T. J. and Chenery S. R. (1995) Laser-ablation ICP-MS elemental analysis of individual fluid inclusions—An evaluation study. *Geochim. Cosmochim. Acta* **59,** 3997–4007.

Shepherd T. J., Ayora C., Cendon D. I., Chenery S. R., and Moissette A. (1998) Quantitative solute analysis of single fluid inclusions in halite by LA-ICP-MS and cryo-SEM-EDS: Complementary microbeam techniques. *Eur. J. Mineral.* **10**(6), 1097–1108.

Shepherd T. J., Naden J., Chenery S. R., Milodowski A. E., and Gillespie M. R. (2000) Chemical analysis of palaeogroundwaters: A new frontier for fluid inclusion research. *J. Geochem. Explor.* **69,** 415–418.

Shibuya E. K., Sarkis J. E. S., Enzweiler J., Jorge A. P. S., and Figueiredo A. M. G. (1998) Determination of platinum group elements and gold in geological materials using an ultraviolet laser ablation high-resolution inductively coupled plasma mass spectrometric technique. *J. Anal. At. Spectrom.* **13**(9), 941–944.

Shimizu N. and Hart S. R. (1982) Applications of the ion microprobe to geochemistry and cosmochemistry. *Earth Planet. Sci. Lett.* **10,** 483–526.

Simon K., Wiechert U., Hoefs J., and Grote B. (1997) Microanalysis of minerals by laser ablation ICPMS and SIRMS. *Fresenius' J. Anal. Chem.* **359**(4–5), 458–461.

Sinton J. A. O. (1999) Volcanological investigations at superfast spreading: Results from R/V Atlantis cruise 3-31. *Ridge Events* **10,** 17–23.

Spandler C. J., Eggins S. M., Arculus R. J., and Mavrogenes J. A. (2000) Using melt inclusions to determine parent-magma compositions of layered intrusions: Application to the Greenhills Complex (New Zealand), a platinum group minerals-bearing, island-arc intrusion. *Geology* **28**(11), 991–994.

Spencer R. J., Moller N., and Weare J. H. (1990) The prediction of mineral solubilities in natural-waters—A chemical-equilibrium model for the Na-K-Ca-Mg-Cl-SO_4-H_2O system at temperatures below 25-degrees-C. *Geochim. Cosmochim. Acta* **54,** 575–590.

Stalder R., Ulmer P., Thompson A. B., and Günther D. (2001) High pressure fluids in the system MgO-SiO_2-H_2O under upper mantle conditions. *Contrib. Mineral. Petrol.* **140**(5), 607–618.

Stirling C. H., Lee D. C., Christensen J. N., and Halliday A. N. (2000) High-precision in situ U^{238}-U^{234}-Th^{230} isotopic analysis using laser ablation multiple-collector ICPMS. *Geochim. Cosmochim. Acta* **64,** 3737–3750.

Suhr G., Seck H. A., Shimizu N., Günther D., and Jenner G. (1998) Infiltration of refractory melts into the lowermost oceanic crust: Evidence from dunite- and gabbro-hosted clinopyroxenes in the Bay of Islands ophiolite. *Contrib. Mineral. Petrol.* **131**(2–3), 136–154.

Sylvester P. (2001a) *Laser-Ablation-ICPMS in the Earth Sciences—Principles and Applications*. Mineralogical Association of Canada.

Sylvester P. (2001b) Trace element analysis of fused whole rock glasses by laser-ablation ICP-MS. In *Short Course Series, Vol. 29* (ed. P. Sylvester), pp. 147–162. Mineralogical Association of Canada.

Sylvester P. (2001c) A practical guide to platinum-group element analysis of sulphides by laser-ablation ICP-MS. In *Short Course Series, Vol. 29* (ed. P. Sylvester), pp. 203–211. Mineralogical Association of Canada.

Sylvester P. J. and Eggins S. M. (1997) Analysis of Re, Au, Pd, Pt and Rh in NIST glass certified reference materials and natural basalt glasses by laser ablation ICP-MS. *Geostand. Newsl.—J. Geostand. Geoanal.* **21**(2), 215–229.

Sylvester P. J. and Ghaderi M. (1997) Trace element analysis of scheelite by excimer laser ablation inductively coupled plasma mass spectrometry (ELA-ICP-MS) using a synthetic silicate glass standard. *Chem. Geol.* **141**(1–2), 49–65.

Tanner S. D. (1995) Characterization of ionization and matrix suppression in inductively-coupled cold-plasma mass-spectrometry. *J. Anal. At. Spectrom.* **10**(11), 905–921.

Tanner S. D. and Baranov V. I. (1999a) A dynamic reaction cell for inductively coupled plasma mass spectrometry (ICP-DRC-MS). II. Reduction of interferences produced within the cell. *J. Am. Soc. Mass Spectrom.* **10**(11), 1083–1094.

Tanner S. D. and Baranov V. I. (1999b) Theory, design, and operation of a dynamic reaction cell for ICP-MS. *At. Spectrosc.* **20**(2), 45–52.

Tanner S. D., Baranov V. I., and Völlkopf U. (2000) A dynamic reaction cell for inductively coupled plasma mass spectrometry (ICP-DRC-MS)—Part III. Optimization and analytical performance. *J. Anal. At. Spectrom.* **15**(9), 1261–1269.

Taylor R. P., Jackson S. E., Longerich H. P., and Webster J. D. (1997) In situ trace-element analysis of individual silicate melt inclusions by laser ablation microprobe inductively coupled plasma-mass spectrometry (LAM-ICP-MS). *Geochim. Cosmochim. Acta* **61,** 2559–2567.

Ulrich T., Günther D., and Heinrich C. A. (1999) Gold concentrations of magmatic brines and the metal budget of porphyry copper deposits. *Nature* **399,** 676–679.

Ulrich T., Günther D., and Heinrich C. A. (2001) The evolution of a porphyry Cu-Au deposit, based on LA-ICP-MS analysis of fluid inclusions: Bajo de la Alumbrera, Argentina. *Econ. Geol.* **96,** 1743–1774.

Valley J. W., Graham C. M., Harte B., Eiler J. M., and Kinney P. D. (1998) Ion microprobe analysis of oxygen, carbon and hydrogen isotope ratios. In *Applications of Microanalytical Techniques to Understanding Mineralizing Processes, Vol. 7* (eds. M. A. McKibben, W. C. Shanks, III, and W. I. Ridley), pp. 73–98. Society of Economic Geologists.

Vanhaecke F., Moens L., Dams R., Allen L., and Georgitis S. (1999) Evaluation of the isotope ratio performance of an axial time-of-flight ICP mass spectrometer. *Anal. Chem.* **71**(15), 3297–3303.

Vanko D. A., Bonnin-Mosbah M., Philippot P., Roedder E., and Sutton S. R. (2001) Fluid inclusions in quartz from oceanic hydrothermal specimens and the Bingham, Utah porphyry-Cu deposit: A study with PIXE and SXRF. *Chem. Geol.* **173**(1–3), 227–238.

Westgate J. A., Perkins W. T., Fuge R., Pearce N. J. G., and Wintle A. G. (1994) Trace-element analysis of volcanic glass shards by laser-ablation inductively-coupled plasma-mass spectrometry—Application to tephrochronological studies. *Appl. Geochem.* **9**(3), 323–335.

Wiechert U. and Hoefs J. (1995) An excimer laser-based micro analytical preparation technique for in-situ oxygen-isotope analysis of silicate and oxide minerals. *Geochim. Cosmochim. Acta* **59,** 4093–4101.

Wilkinson J. J., Rankin A. H., Mulshaw S. C., Nolan J., and Ramsey M. H. (1994) Laser ablation-ICP-AES for the determination of metals in fluid inclusions—An application to the study of magmatic ore fluids. *Geochim. Cosmochim. Acta* **58,** 1133–1146.

Williams I. S. (1998) U-Th-Pb geochronology by ion microprobe. In *Applications of Microanalytical Techniques to Understanding Mineralizing Processes, Vol. 7* (eds. M. A. McKibben, W. C. Shanks, III, and W. I. Ridley), pp. 1–35. Society of Economic Geologists.

Willigers B. J. A., Baker J. A., Krogstad E. J., and Peate D. W. (2002) Precise and accurate in situ Pb-Pb dating of apatite, monazite, and sphene by laser ablation multiple-collector ICP-MS. *Geochim. Cosmochim. Acta* **66,** 1051–1066.

Wollenweber D., Strassburg S., and Wunsch G. (1999) Determination of Li, Na, Mg, K, Ca and Fe with ICP-MS using cold plasma conditions. *Fresenius' J. Anal. Chem.* **364**(5), 433–437.

Zalm P. C. (2000) Dynamic SIMS. Quantification at all depths? *Mikrochim, Acta* **132**(2–4), 243–257.